Mineralogical and elemental geochemical characteristics of Taodonggou Group mudstone in Taibei Sag, Turpan-Hami Basin: Implication for its formation mechanism

Huan Miao[1,2*], Jianying Guo[3*], Yanbin Wang[4], Zhenxue Jiang[1,2], Chengju Zhang [1,2], Chuanming Li[1,5]

[1]State Key Laboratory of oil and gas resources and exploration, Beijing 102249, China;

[2]Institute of unconventional oil and gas science and technology, China University of Petroleum (Beijing), Beijing 102249, China;

[3] CNPC Key Laboratory of Natural Gas Accumulation and Development,Langfang 065007,China;

[4]School of Geosciences and Surveying Engineering,China University of Mining and Technology(Beijing),Beijing 100083,China;

[5]College of Geosciences, China University of Petroleum (Beijing), Beijing 102249, China;

Correspondence to: Huan Miao(1627765379@qq.com); Jianying Guo (gjy_17711224@petrochina.com.cn)

Abstract. Organic matter types in the Taodonggou Group mudstone exhibit significant differences with depth. In order to understand the formation mechanism of this special phenomenon, we analyzed the mineralogy and geochemistry of the mudstone, as well as the source rocks, depositional environment, and depositional processes of the Taodonggou Group. Based on this, we have gained the following understanding: (1) The Taodonggou Group mudstone was deposited in an intermediate-depth or deep, dyoxic, freshwater-brackish lake environment under warm and humid paleoclimatic conditions. The input of terrestrial debris was stable, but the sedimentation rate was slow. In addition, the sedimentation in the middle stage was influenced by hydrothermal activities, and the changes in the depositional environment corresponded to variations in organic matter types. (2) The source rocks of the Taodonggou Group mudstone are mainly andesitic and feldspathic volcanic rocks. Sediment sorting and recycling were weak, and hydrocarbon source information was well preserved. The tectonic background of the source area was a continental island arc and an oceanic island arc. Furthermore, changes in the provenance of the Taodonggou Group also had a significant impact on the variations in organic matter types. (3) The sedimentation of the Taodonggou Group involved both traction and gravity flows. The variations in source area, depositional environment, and depositional processes during different depositional periods led to changes in the organic matter types of the Taodonggou mudstone. (4) Based on the depositional environment, provenance, and depositional processes, the sedimentation of the Taodonggou Group can be divided into three stages. In the early stages, the sedimentation center was in the Bogda area. At this time, the Bogda Mountain region was not exposed, and the depositional processes inherited the characteristics of Early Permian gravity flow sedimentation, resulting in the widespread deposition of a series of high-quality Type III source rocks in the basin. In the middle stage of the Taodonggou Group sedimentation, the sedimentation center gradually migrated to the Taibei Sag. During this period, the Bogda Mountain region experienced uplift and hydrothermal activity, and the depositional processes gradually transitioned to traction flows, resulting in the widespread deposition of a series of Type II source rocks in the basin. In the late stage of the Taodonggou Group, the uplift of the Bogda Mountain region ceased, and the sedimentation

center completely shifted to the Taibei Sag. Meanwhile, under the influence of gravity flows, the organic matter types of the Taodonggou mudstone changed to Type III.

Keyword: Turpan-Hami Basin;Taodonggou Group;Mineralogy;Element Geochemistry;Sedimentary Environment; Source sink system

1 Introduction

Turpan-Hami Basin, Junggar Basin and Bogda area all belong to the southern part of the ancient Asian ocean in the Paleozoic era (Korobkin and Buslov, 2011; Jiang et al., 2015). During the Early Carboniferous to Early Permian, they began momentously to separate due to the continuous expansion of the Bogda Rift and began to enter the basin-forming period in the Middle Permian (Miao et al., 2004; Novikov, 2013; Jiang et al., 2015; Wang et al., 2019; Zhang et al., 2019). The Middle Permian is a momentous stage in the tectonic evolution of the Turpan-Hami basin. During this period, the expansion of the Bogda Rift stopped. With the gradual withdrawal of seawater from Xinjiang, the sedimentary environment of the Turpan-Hami basin gradually shifted to continental facies, and the sedimentary center gradually shifted from the Bogda area to Taibei Sag (Miao et al., 2004; Shi et al., 2020; Li et al., 2022). Taodonggou Group mudstones are widely deposited in the Turpan-Hami Basin. Previous studies have confirmed that Taodonggou Group mudstone is a very good to excellent source rock with huge hydrocarbon generation potential (Song et al., 2018; Miao et al., 2021; Miao et al., 2022; Miao et al., 2022a). It has been found that the organic matter types of the Taodonggou mudstone can be classified into two categories, with the upper and lower sections being Type III and the middle section being Type II (Miao et al., 2021; 2023).

The hydrocarbon generation potential of mudstone is closely related to its sedimentary environment (Wu et al., 2021; Li et al., 2022; Zhang et al., 2019; Zhao et al., 2021; Miao et al., 2004). Regarding the sedimentary environment of the Taodonggou Group mudstone, previous researchers have conducted extensive research. Miao et al. (2004) believed that the mudstone in the Taodonggou Group was deposited in a warm and humid paleoclimate, high-salinity water bodies, and an anoxic environment. Yang et al. (2010), based on the sedimentary characteristics of the Taerlang Formation and the Daheyan Formation, believed that the Taodonggou Group was deposited in a subhumid climate and that climate change is periodic. Wei (2015) also confirmed that the paleoclimate change of the Taodonggou Group stratum has a cyclical feature through tree rings and is mainly a warm and humid paleoclimate. At the same time, Song et al. (2018) also confirmed this by using the elemental geochemical characteristics of the Taodonggou Group shale outcrops in the field; Tian et al. (2017) analyzed the biomarkers of the Taodonggou Group in 7 outcrops around the Turpan-Hami Basin and concluded that the mudstone of the Taodonggou Group was deposited in a balanced, filled lake with little or no terrestrial organic matter, a large amount of algal organic matter input, and weakly alkaline, hypoxic to hypoxic brackish water. Miao et al. (2021) found biomarkers in the Taodonggou Formation mudstone from wells YT1 and L30 from different perspectives of Tian, which may be related to the

weathering effect of outcrop samples. Through the research of the above scholars, we have found that there is some controversy over the sedimentary environment of the Taodonggou Group, and the relationship between the cyclic changes in the sedimentary environment and the changes in the organic matter types of the Taodonggou Group mudstone is still unclear.

In addition, the provenance and sedimentation mode of sediments also have a significant influence on the organic matter types in mudstones (Mei et al., 2020). Mudstone belongs to a category of fine-grained sediment that is challenging to analyze using traditional heavy mineral analysis methods (Rollinson, 1993; Roser and Korsch, 1988; Gehrels et al., 2008). Therefore, elemental geochemical methods can be employed for provenance analysis (McLennan et al., 1983; Kröner et al., 1985; Li et al., 2020). Elemental geochemical analysis compares the major, trace, and rare earth element characteristics of mudstones in the sedimentary area with those of lithologies in the provenance area to determine the lithology of source rocks, weathering degree, and tectonic background of the sediment source area (Li et al., 2020; Floyd and Leveridge, 1987; Basu et al., 2016). Previous studies have found that the sediment source not only affects variations in the salinity of lake water but also influences the input of nutrients and terrestrial organic matter, thus impacting the quality of mudstones (Li et al., 2020; Deditius, 2015; Essefi, 2021). The tectonic activity in the source area not only affects changes in the sedimentary center but also influences the source area (Miao et al., 2022b; Pinto et al., 2010). Therefore, reconstructing the location and sedimentation mode of the sediment source area is of great significance for understanding the variations in organic matter types in the Taodonggou Group mudstones.

Based on the mineralogical and elemental geochemical characteristics of 16 mudstone samples collected from the YT1 well, this study aims to reconstruct the paleoclimatic features, provenance, and tectonic background of the sedimentary period in the source area of the Taodonggou Group mudstones. It also aims to explore the influence of sedimentary environment, provenance changes, and sedimentation mode on the deposition of the Taodonggou Group mudstones, in order to reveal the formation process of the mudstones.

2 Geological setting

The Turpan-Hami Basin, located in the eastern part of Xinjiang Uygur Autonomous Region, is one of the three major petroliferous basins in Xinjiang. It is 660 km long from east to west and 130 km wide from north to south, with a total covered area of 5.35×104 km². The Turpan-Hami Basin has undergone four stages: the extensional rift basin development stage, the compressional foreland basin development stage, the extensional faulted basin development stage, and the compressional regenerated foreland basin development stage, which finally formed the current pattern of the Mesozoic-Cenozoic superimposed composite inland basin (Zhu et al., 2009; Jiang et al., 2015; Wartes et al., 2002; Greene et al., 2005). According to the tectonic evolution characteristics of the Turpan-Hami Basin, the Turpan-Hami Basin can be divided into three primary tectonic units from east to west: the Hami Depression, the Liaodun Uplift, and the Turpan Depression (Miao et al., 2021; Fig. 1a).

94   Taibei sag, the secondary sag of Turpan depression in Turpan-Hami basin, is the largest sedimentary unit in Turpan-Hami

95   basin (Fig. 1b). The Taibei sag is a Paleozoic-Cenozoic inherited subsidence area (Li et al., 2021), which is a key area for oil

96   and gas exploration in the Turpan-Hami Basin due to its high thermal evolution degree of hydrocarbon source rocks, good

97   reservoir physical properties, good cap sealing, and rich oil and gas resources, which are the focus of oil and gas exploration

98   in the Turpan-Hami Basin. (Wu et al., 2021; Li et al., 2021). Taodonggou Group is the general name of the Daheyan Formation

99   and the Taerlang Formation. The Daheyan Formation is composed of a sequence of sandstone and conglomerate deposits,

100 with locally interbedded gray to dark gray mudstone. It is unconformably overlain by the Yierxitu Formation. The Taerlang

101 Formation is predominantly composed of gray-black mudstone, with localized occurrences of gray-green siltstone and

102 medium-grained sandstone. Due to the fact that the stratigraphic boundary between the Taerlang Formation and the Daheyan

103 Formation is not obvious, they are collectively called the Taodonggou Group. The Middle Permian Taodonggou Group is

104 mainly located in the western part of the study area. At present, only the YT1 and L30 wells are drilled (the YT1 well is drilled

105 through; the L30 well is not drilled through). The burial depth of the stratum is 4000–6500 m, and the thickness of the

106 mudstone is 50–200 m (Miao et al., 2022b).

3 Samples and experiments

3.1 Samples

109 In this study, 16 mudstone samples were collected from well YT1, numbered YT1-1 to YT1-16 in order of depth. After

110 cleaning the samples, XRD, XRF and ICP-MS experiments were conducted.

3.2 Experiments

112 The XRD experiment was carried out at Hangzhou Yanqu Information Co., Ltd. The experimental instrument was the

113 Ultima VI XRD testing instrument of Japanese Neo-Confucianism. In accordance with the Chinese industry standard SY/T

114 5163-2018, the mudstone was broken to a particle size of less than 200 meshes, and 2 g of samples were weighed to obtain

115 XRD images through Cu/Ka radiation at a scanning speed of 2 °/min. The measurement angle range was $3° \leq 2\theta \leq 70°$, and

116 finally, quantitative interpretation is made with the software X'Pert Highscore Plus of Panalytic Company.

117 The XRF experiment was conducted in Hangzhou Yanqu Information Co., Ltd., and the experimental instrument was a

118 Panalytical Axios tester from Panalytical. The mudstone was first crushed to a particle size of less than 200 meshes, then 10

119 g of the sample was weighed and calcined in a muffle furnace for 4 hours to get rid of organic matter and carbonates, weighed

120 and recorded the weight loss, and finally $Li_2B_4O_7$ was added, mixed evenly and made into glass bead, and the main element

121 concentration was tested.

122 The ICP-MS test was performed at Beijing Orient Smart, and the test instrument was an ELEMENT XR inductively

123 coupled plasma emission spectrometer manufactured by Thermo Fisher, Inc. Before analysis, the samples were ground to a

124 particle size of less than 40 μm. An appropriate amount of the sample was weighed and dissolved in HF (30%) and HNO3

125 (68%) at 190°C for 24 hours. After evaporating the excess solvent with deionized water, the solution was redissolved in 2 ml

126 of 6.5% HNO_3. Redissolve in 2 ml of 6 mol/L HNO_3 and then store at 150 °C for 48 hours. Subsequently, after evaporating

127 the solution, 1 ml of the 6 mol/L HNO_3 evaporated solution was added to the sample.

4 Results

4.1 Mineralogy

130 The XRD test results of 16 samples from Well YT1 are shown in Table 1 and Figure 2. As can be seen from Table 1 and

131 Figure 2, Taodonggou Group mudstones are composed of clay, quartz, calcite, plagioclase, barite, and K-feldspar, and some

132 samples contain siderite and pyrite. The content of clay is the highest (23.9%–70.9%, mean 40.78%), followed by quartz

133 (17.2%–59.2%, mean 34.69%), calcite (1%–35.4%, mean 16.97%), barite (0%–13.3%, mean 4.21%), plagioclase (0%–5.4,

134 mean 2.93%), and K-feldspar (0%–2.3, mean 0.9%).

135 The mineral composition can be used to analyze the lithofacies type of mudstone, and different lithofacies types often

136 have different characteristics (Glaser et al., 2014). Previous scholars believed that mudstone types could be divided by the

137 ternary diagram of mineral composition. The three end elements of the ternary diagram are quartz + feldspar + mica (QFM),

138 calcite + dolomite + ankerite + siderite + magnesite (carbonate), and clay. The XRD results of 16 mudstone samples from

139 Well YT1 in the study area are put into the ternary map (Fig. 3). The results show that the data points of Taodonggou Group

140 mudstone in the study area are located in four areas, namely, mixed mudstone, silica-rich argillaceous mudstone, argillaceous

141 siliceous mudstone and mixed siliceous mudstone, and most of the points are mixed mudstone and argillaceous siliceous

142 mudstone areas, which indicates that Taodonggou Group mudstone can be divided into four types: mixed mudstone, silica-

143 rich argillaceous mudstone, argillaceous siliceous mudstone and mixed siliceous mudstone, and the main lithofacies are mixed

144 mudstone and argillaceous siliceous mudstone.

4.2 Major element

146 Table 2 shows the results of the major elements in 16 mudstone samples from Well YT1. From Table 2, we can see that

147 the major elements of the Taodonggou Group mudstone are mainly SiO_2, Al_2O_3, Fe_2O_3, CaO, and TiO_2. The highest content

148 of SiO_2 is from 43.11% to 70.11%, with an average value of 56.18%. Al_2O_3 content takes second place, accounting for 11.65%

149 to 25.75%, with an average value of 18.69%; the average content of another main element is less than 10%.

4.3 Trace element

151 The trace element content of the Taodonggou Group mudstone is shown in Table 3. Enrichment factor (EF) is an

152 important indicator of element enrichment (Taylor and McLennan, 1985; Ross and Bustin, 2009). By comparing the trace

153 element content of the mudstone of the Taodonggou Group with the global average shale (AS), the trace element enrichment

154 factors in the study area are calculated as follows:

155
$$X_{EF} = \frac{(X / Al)_{samples}}{(X / Al)_{AS}} \qquad (1)$$

156 Where X and Al represent the concentrations of elements X and Al (Taylor and McLennan, 1985; Ross and Bustin, 2009).

157 X_{EF} < 1 represents the dilution concentration of element X relative to the standard composition, X_{EF} > 1 represents the relative

158 enrichment of element X compared to the AS concentration, X_{EF} > 3 represents the detectable autogenetic enrichment, and

159 X_{EF} > 10 is considered an indicator of moderate to strong autogenetic enrichment (Taylor and McLennan, 1985; Ross and

160 Bustin, 2009).

161 Figure 4 and Table 4 presents the enrichment factors of Taodonggou Group mudstone in the study area. It can be seen

162 from Figure 4 and Table 4 that only Hf (0.5-2.11, mean = 1.29) is enriched in the Taodonggou Group mudstone compared

163 with AS, and other elements are no enriched.

4.4 Rare earth element

165 The REE content of Taodonggou Group mudstone in the study area is shown in Table 5. According to Table 5, the ∑REE

166 content of Taodonggou Group mudstone ranged from 43.247 ppm to 257.997 ppm, with an average value of 159.206 ppm.

167 The light rare earth element (LREE) content was the highest (mean value 133.45 ppm), followed by medium rare earth element

168 (MREE) (mean value 17.438 ppm) and heavy rare earth element (HREE) (mean value 6.684 ppm) in that order. After chondrite

169 standardization (Taylor and Mclennan, 1985), Taodonggou Group mudstone shows a right dipping REE distribution pattern

170 (Fig. 5), (La/Yb) $_N$ is 6.228–10.081, with an average value of 7.358.

171 In addition, in Figure 5, although the YT1-13 sample exhibits a weak right dipping REE distribution pattern similar to

172 other samples, its rare earth elements are significantly depleted. Based on Figure 4 and Table 4, the trace elements in the YT1-

173 13 sample are depleted compared to AS, indicating that the YT1-13 sample has been influenced by groundwater leaching.

4.5 Reconstruction of paleosedimentary environment based on element geochemical characteristics

175 4.5.1 Paleoclimate and weathering

176 The paleoclimate not only affects the weathering degree of the parent rock but also affects the transport distance of

177 sedimentary debris and the transport of nutrients (Zhang et al., 2005). There are many evaluation indices for paleoclimate,

178 such as the chemical alteration index (CIA) and the climate index (*C*). It is generally believed that when CIA=50–65 and *C* <

179 0.2, it reflects that the sedimentary system is in a dry and cold climate under the background of lower of degree of chemical

180 weathering; when CIA=65–85 and 0.2 < *C* < 0.8, it indicates that the sedimentary system is in a warm and humid climate

181 under the background of middle of degree of chemical weathering; when CIA=85–100 and *C* > 0.8, it reflects the humid and

182 hot climate under the background of high of degree of chemical weathering (Zhang et al., 2019; Nesbitt and Young, 1984).

183 The calculation formula for CIA and C is as follows:

184
$$CIA = \frac{Al_2O_3 \times 100}{Al_2O_3 + Na_2O + CaO* + K_2O} \qquad (2)$$

185
$$C = \frac{Fe + Mn + Cr + Ni + V + Co}{Ca + Mg + Sr + Ba + K + Na} \qquad (3)$$

186 In formula (2), CaO * only refers to CaO in silicate minerals. Due to the lack of direct measurement means, it is often

187 calculated indirectly by the content of P_2O_5, namely:

$$188 \qquad CaO* = mol(CaO) - \frac{10}{3}mol(P_2O_5) \qquad\qquad\qquad\qquad\qquad (4)$$

189   Where, mol(CaO) and mol(P_2O_5) are the mole numbers of CaO and P_2O_5, where when mol (Na_2O) ≤ mol (Cao *), mol

190   (Ca0 *) = mol (Na_2O); on the contrary, when mol(Na_2O) > mol(CaO*), mol(CaO*)=mol(CaO) (Nesbitt and Young, 1984).

191   The CIA values of the Taodonggou Group mudstone in the study area were calculated based on Equation (2) and Equation

192   (3), ranging from 68.71 to 96.97, with a mean value of 80.17. The climate index (*C*) is 0.22–2.42 (average = 1.01, Tab.3). The

193   overall paleoclimate was warm, humid, and hot (Fig. 6a).

194   In addition, the cross plot of Ga/Rb and K_2O/Al_2O_3 can also be used to analyze the paleoclimate characteristics during

195   the formation of sedimentary rocks (Lerman and Baccini, 1987; Liu and Zhou, 2007). As shown in the cross plot of Ga/Rb

196   and K_2O/Al_2O_3 (Fig. 6b), almost all points are in the warm/wet area, which indicates that Taodonggou Group mudstone was

197   deposited in a warm and humid paleoclimate.

198   By analyzing the correlations between CIA, *C*, and Ga/Rb (Figure 6c–e), it can be observed that there is the strongest

199   correlation between CIA and *C* (Figure 6c, R^2 = 0.7566). Additionally, the correlation coefficients between CIA and Ga/Rb,

200   as well as *C* and Ga/Rb, are both greater than 0.4 (Figures 6d and 6e). This indicates that CIA, *C*, and Ga/Rb are reliable

201   indicators of the paleoclimate during the sedimentation of the Taodonggou Group mudstone. Based on the above analysis, the

202   Taodonggou Group mudstone in the study area was deposited in a warm, humid, and hot paleoclimate. This result is consistent

203   with Miao's indicator result using the biomarker parameter CPI (Miao et al., 2021), indicating that the biomarker parameter

204   CPI can be used to explain the paleoclimate change characteristics of hydrocarbon source rocks with Ro ≤ 1.49.

205   4.5.2 Paleo-redox conditions

206   Redox environments are critical to the preservation of organic matter in sedimentary rocks, and sensitive elements such

207   as Co, Mo, U, Th, V, Ni, and Cr are commonly used to identify redox conditions in ancient water bodies. Previous evidence

208   suggests that U/Th < 0.75, V/Cr < 2 and V/(V+Ni) < 0.45 represent an oxic conditions, 0.75 < U/Th < 1.25, 2 < V/Cr < 4.25

209   and 0.45 < V/(V+Ni) < 0.84 represent a dyoxic conditions, U/Th < 1.25, V/Cr < 4.25 or V/(V+Ni) < 0.84 represent an anoxic

210   condition (Hatch and Leventhal, 1992; Rosenthal et al., 1995; Tribovillard et al, 2006; Tribovillard et al, 2012). There is no

211   significant correlation between V, U, and Th and Al_2O_3 contents in the Taodonggou Group mudstone samples, indicating that

212   V, U, and Th contents in Taodonggou Group mudstone are mainly controlled by authigenic deposition under redox conditions

213   (Tribovillard et al., 1994). The U/Th, V/Cr, and V/(V+Ni) of the Taodonggou Group mudstone range from 0.21 to 0.52 (mean

214   = 0.29), 1.62 to 4.95 (mean = 2.7), and 0.65 to 0.92 (mean = 0.75). In the light of U/Th, Taodonggou Group mudstones were

215   deposited in an oxic environment, and according to V/Cr and V/(V+Ni), Taodong Group mudstones were deposited in a

216   dyoxic environment. This is because U/Th cannot accurately identify the redox environment of the sediments under highly

217   weathered conditions (Cao et al., 2021), so V/Cr and V/(V+Ni) were used in this study to identify the redox environment of

218   Taodonggou Group mudstone. The cross plot of V/Cr and V/(V+Ni) shows (Fig. 7) that Taodonggou Group mudstones were

219   deposited in a dyoxic environment.

220   4.5.3 Paleosalinity

221   Paleosalinity is an important indicator of the paleoenvironment of a water body. The level of paleosalinity affects the

222   stratification of the sedimentary water body and the development of plankton, thereby affecting the paleoproductivity and

223   enrichment of organic matter in the sedimentary environment (Thorpe et al., 2012; Wang et al., 2021; Shi et al., 2021).

224   Previous research has found that Sr/Ba and B/Ga can represent changes in paleosalinity. It is generally believed that Sr/Ba<0.5

225   or B/Ga<3 represents fresh water, 0.5<Sr/Ba<1 or 3<B/Ga<6 means brackish water, and Sr/Ba>1 or B/Ga>6 represents saline

226   water. The correlation between Sr and CaO of Taodonggou Group mudstone in the study area is not obvious (R^2=0.17), Sr/Ba

227   of Taodonggou Group mudstone in the study area ranges from 0.32 to 1.83, with an average value of 0.71, and the B/Ga is

228   2.53–5.81 (average = 3.36), indicating that Taodonggou Group mudstone was deposited in freshwater and brackish water

229   environments (Fig. 8a).

230   In addition, Ca/(Ca+Fe) is a reliable indicator for evaluating the salinity of lake waters (Wang et al., 2021). The

231   Ca/(Ca+Fe) distribution of Taodonggou Group mudstone in the study area ranges from 0.14 to 0.78, with a mean value of

232   0.42. The Sr/Ba and Ca/(Ca+Fe) intersection diagram (Fig. 8 b) shows that Taodonggou Group mudstones were deposited in

233   freshwater and brackish water environments, which is in accord with the Sr/Ba and B/Ga intersection diagram.

234   4.5.4 Paleobathymetry

235   Previous research has shown that some elements of the sedimentation process change dramatically with offshore distance.

236   These elements can be used to judge the water depth variation during the sedimentation period. The commonly used indicators

237   are Zr/Al, Rb/K, and MnO content (Xiong and Xiao, 2011; Herkat et al., 2013). It is now believed that the lower the Zr/Al

238   ratio or the higher the Rb/K ratio, the further offshore and the deeper the water (Xiong and Xiao, 2011; Herkat et al., 2013).

239   Zr/Al of Taodonggou Group mudstone is 5.19×10^{-4}– 22.51×10^{-4} (average = 13.44×10^{-4}), showing a trend of first decreasing

240   and then increasing with the depth, Rb/K ranges from 7.32×10^{-4} to 29.79×10^{-4} (mean 19.02×10^{-4}), with large fluctuations

241   with depth of burial. The high-value area of Rb/K is basically consistent with the low-value area of Zr/Al, which indicates

242   that the ancient water depth during the Taodonggou Group mudstone deposition process has a trend of first decreasing and

243   then increasing.

244   For the content of MnO, it is generally believed that < 0.00094% is a shore lake, 0.00094%–0.0075% is a shallow lake,

245   0.0075%–0.051% is an intermediate-depth lake, and > 0.051% is a deep lake (Herkat et al., 2013). MnO of Taodonggou Group

246   mudstone is 0.05%–0.30%, with an average of 0.16 %, which indicates that the Taodonggou Group mudstone are mainly

247   deposited in intermediate depth - deep lake sedimentary environment.

248   4.5.5 Terrigenous detritus input

249   Ti, Si, and Al are relatively stable during diagenesis and are usually used as indicators of debris flux input (Algeo and

Maynard, 2004; Maravelis et al., 2021). Generally, Ti in sediments comes from ilmenite ($FeTiO_3$) or rutile (TiO_2), while Al can exist in feldspar, clay minerals, and other aluminum silicate minerals (Algeo and Maynard, 2004). Compared with Ti and Al, Si comes from many sources, including both biological origin and hydrothermal and terrigenous clastic input (Kidder and Erwin, 2001). Therefore, when using SiO_2 as the evaluation index for terrigenous clastic input, its source needs to be analyzed. The correlation of Al_2O_3 and TiO_2 with SiO_2 in Well YT1 of the study area is not obvious, which indicates that their sources are more complex and not dominated by terrestrial debris sources (Fig. 9). Therefore, Al_2O_3 and TiO_2 are used in this study to indicate the terrestrial debris input during the deposition of the Taodonggou Group mudstone.

The Al_2O_3 content of YT1 wells is higher, ranging from 11.65 % to 25.75 %, with an average value of 18.69 %; the TiO_2 is 1.15 %–4.22 % (average = 1.77 %). As can be seen from Table 2, the Al_2O_3 content of Well YT1 fluctuates more with depth, and the overall trend is increasing first and then decreasing with depth, while the TiO_2 fluctuates less with depth, and on the whole, the trend is increasing with depth. Combined with the results of paleoclimate analysis in the study area, it is found that the terrestrial debris input during the deposition of the Taodonggou Group strata has the characteristics of increasing first and then decreasing.

4.5.6 Paleoproductivity

Paleoproductivity determines the quantity of original organic matter in sedimentary rocks (Wei et al., 2012; Algeo and Ingall, 2007; Ross and Bustin, 2009; Schoepfer et al., 2015). The elements P, Si, Ba, Zn, and Cu are indicators of the magnitude of paleoproductivity, but they all have a certain range of application; for example, only the biogenic parts of Si and Ba can represent productivity, and Zn can only represent productivity change in the sulfide reduction environment (Wei et al., 2012; Algeo and Ingall, 2007).

P is not only a key nutrient element in biological metabolism but also an important component of many organisms, so it can also be used to characterize biological productivity (Kidder and Erwin, 2001). P/Ti or P/Al is commonly used to reflect biological productivity in order to eliminate the influence of terrigenous detritus. The P/Ti of Taodonggou Group mudstone in the study area ranges from 0.04 to 0.74 percent, with an average value of 0.17 percent and an overall low productivity. As shown in Table 2, the relationship between P/Ti and depth was analyzed, and the results showed that the paleontological productivity tended to increase and then decrease with depth.

In addition, Cu is also an important nutrient and, unlike P, is generally indicative of productivity, including the sum of primary productivity and productivity from terrestrial inputs (Schoepfer et al., 2015). For the purpose of eliminating the dilution interference of terrigenous detritus, Cu/Ti is used as an indicator to evaluate the paleoproductivity in this study. The distribution range of Cu/Ti of Taodonggou Group mudstone in the study area is from 0.55 to 1.96 with an average value of 1.02 and gradually decreases with depth, indicating a gradual increase in palaeoproductivity during the deposition of Taodonggou Group mudstone.

4.5.7 Deposition rate

The deposition rate is one of the parameters characterizing the magnitude of the dilution effect during deposition and is commonly characterized by $(La/Yb)_N$. It is generally believed that the difference between LREE and HREE migration is not significant when the sedimentation rate of the lake basin is faster and the $(La/Yb)_N$ value is close to 1. Conversely, when the $(La/Yb)_N$ value is greater or less than 1, it indicates that the sedimentation rate of the lake basin is slower (Wang et al., 2021; Cao et al., 2018). The $(La/Yb)_N$ of the Taodonggou Group mudstones are 6.228–10.081, with an average value of 7.358 in the study area, which is much greater than 1. This indicates that the mudstone of the Taodonggou Group has a slower deposition rate.

4.5.8 Hydrothermal activity

The study area has been extremely volcanically active from the Carboniferous to the Permian, with extensive volcanic deposits in the Middle Permian Taodongou Group, the Lower Permian Yierxitu Formation, and the Carboniferous. In order to explore whether hydrothermal activity is involved in the Middle Permian sedimentation, the Zn-Ni-Co ternary diagram and the $(Cu+Co+Ni)\times10$-Fe-Mn ternary diagram are applied in this study (Xu et al., 2022; You et al., 2019). Based on the Zn-Ni-Co ternary diagram (Fig. 10a), some data points of the Taodonggou Group mudstone are distributed in the hydrothermal sedimentary zone, and based on the $(Cu+Co+Ni)\times10$-Fe-Mn ternary diagram (Fig. 10b), all data points of the samples fall in the hydrothermal sediment zone and Red Sea hydrothermal sediment zone, which indicates that the Taodonggou Group mudstone deposition was influenced by hydrothermal fluids.

4.5.9 Tectonic setting

Sedimentary rocks of different tectonic settings have prominent differences in element composition and content, so the geochemical characteristics of sedimentary rocks can be used to reflect the tectonic setting of sedimentary basins (Kroonenberg, 1992).

The elements Co, Th, Sc, Zr, and La are relatively stable and less affected by geological activities such as weathering, transportation, and deposition. Therefore, the La-Th-Sc ternary diagram and the Th-Co-Zr/10 ternary diagram can be utilized to distinguish the tectonic setting during the formation of sediments (Bhatia and Crook, 1986; Cai et al., 2022). Based on the La-Th-Sc ternary diagram (Fig. 11a), most of the data points fall in the continental island arc region, and on the Th-Co-Zr/10 ternary diagram (Fig. 11b), almost all the data points fall in the continental island arc and oceanic island arc regions. This indicates that the tectonic setting of the Taodonggou Group's source area is a continental island arc and an oceanic island arc.

Additionally, previous studies have shown that SiO_2, TiO_2, Al_2O_3/SiO_2 and Fe_2O_3+MgO are also important parameters for identifying the source tectonic setting. Cross plots of Al_2O_3/SiO_2 and Fe_2O_3+MgO, TiO_2 and Fe_2O_3+MgO, and SiO_2 and Al_2O_3/SiO_2 are often employed to recognize the tectonic setting (Bhatia, 1983; Li et al., 2020; Roser and Korsch, 1988). Based on the cross plot of Al_2O_3/SiO_2 and Fe_2O_3+MgO (Fig. 11c), all data points are distributed around the continental island arc

312 and oceanic island arc, which is consistent with the cross plot of TiO_2 and Fe_2O_3+MgO (Fig. 11d) and the cross plot of SiO_2

313 and Al_2O_3/SiO_2 (Fig. 11e). As a result, the tectonic setting of Taodonggou Group mudstone source area is continental island

314 arc and oceanic island arc.

5 Discussion

316   The sedimentary environment, provenance location, and sedimentation mode are factors that influence the quality of

317 mudstones. In this study, based on the mineralogical and elemental geochemical characteristics of the Taodonggou Group

318 mudstones, we discuss the influence of sedimentary environment, provenance location, and sedimentation mode on the quality

319 of the Taodonggou Group mudstones.

5.1 The influence of palaeosedimentary environment on the quality of mudstone

321   Based on the mineralogical, elemental geochemical characteristics and previous studies on the organic geochemical

322 characteristics of the Taodonggou Group mudstones (Miao et al., 2021), a comprehensive geochemical profile of the YT1

323 well was established. The results are shown in Figure 12. It can be observed from Figure 12 that the sedimentary environment

324 of the Taodonggou Group mudstones is closely related to their organic matter types and can be divided into three periods. In

325 the early stage of the Taodonggou Group, the overall climate was warm and humid under moderate chemical weathering

326 conditions. The sedimentary water body was dyoxic-anoxic brackish water. At this time, productivity was weak, and organic

327 matter was mainly derived from terrestrial sources. In the middle stage of the Taodonggou Group, the paleoclimate gradually

328 shifted to a dry and humid climate under strong chemical weathering conditions, accompanied by hydrothermal activity. This

329 provided abundant nutrients for the growth of algae and other microorganisms. At the same time, the sedimentation rate

330 increased, resulting in a predominance of algae in the organic matter composition during this period. During the late stage of

331 the Taodonggou Group, the climate again shifted to a warm and humid climate under moderate chemical weathering

332 conditions. The sedimentation rate slowed down, and the input of organic matter shifted back to predominantly terrestrial

333 sources.

5.2 Provenance

335 5.2.1 Lithology of parent rock

336   Previous studies have found that the chemical composition of the rocks in the sedimentary area and the parent rock in

337 the provenance area have a strong affinity, and the type of parent rock will directly affect the elemental geochemical

338 characteristics of the sediment (Tribovillard et al., 2006; Shi et al., 2021; McLennan et al., 1993; Basu et al., 2016; Hu et al.,

339 2021; Floyd and Leveridge, 1987; Wronkiewicz and Condie, 1987). Generally speaking, the transport of sediment from the

340 source area to the sedimentary area goes through multiple complex processes such as mechanical transport and chemical

341 action, and hence it is necessary to analyze the impact of sediment sorting and recycling on each chemical component when

342 identifying the source. Previous studies have shown that trace elements Zr, Th, and Sc are relatively stable in geological

343 processes such as weathering, transportation, and sorting and are not easily lost, which can be used as one of the indicators

344 for parent rock identification (Floyd and Leveridge, 1987; Wronkiewicz and Condie, 1987). According to the Th/Sc and Zr/Sc

345 intersection diagram of Taodonggou Group mudstone (Fig. 13a), Taodonggou Group mudstone is close to andesite and felsic

346 volcanic rock of the upper crust, and its composition is controlled by the composition of its felsic parent rock and has not

347 undergone sediment sorting and recycling.

348 In addition, REE and trace elements in mudstone from different parent rocks are obviously different, so the ratio of REE

349 to trace elements can be used to analyze the type of parent rock, and the most common ones are La/Sc, La/Co, Th/Sc, Th/Co,

350 and Cr/Th (Basu et al., 2016; Hu et al., 2021; Floyd and Leveridge, 1987; Wronkiewicz and Condie, 1987; Allègre and Minster,

351 1978). Based on the Hf and La/Th intersection diagrams (Fig. 13b) and the La/Sc and Co/Th intersection diagrams (Fig. 13c),

352 we can see that the mudstones of the Taodonggou Group have both andesitic island-arc sources and felsic volcanic sources.

353 It can be seen from the cross plot of TiO_2 and Zr (Fig. 13d) that the mudstone of the Taodonggou Group is a source of

354 intermediate igneous rocks and felsic igneous rocks. As can be seen from the cross plot of La/Yb and Σ REE (Fig. 13e), almost

355 all data points are located in the sedimentary rock, alkali basalt, and granite areas.

356 In summary, the parent rocks of the Taodonggou Group mudstone are andesitic and feldspathic volcanic rocks with weak

357 sedimentary sorting and recirculation, and the material source information is well preserved.

358 5.2.2 Location of Parent Rock

359 There is a great deal of controversy about the provenance location of the Middle Permian in Turpan-Hami (Shao et al.,

360 2001; Jiang et al., 2015; Wang et al., 2019; Zhao et al., 2020; Song et al., 2018; Wang et al., 2018; Tang et al., 2014). Shao et

361 al. (1999) believed that the provenance of the Permian was mainly from the Jueluotage Mountain in the south of the Turpan-

362 Hami Basin; Song et al. (2018) considered that it came from the Bogda area; Zhao et al. (2020) believed that the provenance

363 of the Permian in the Turpan-Hami Basin was consistent with that in Junggar and originated from the Kelameili Mountain

364 and the Northern Tianshan. Summarizing the previous research results, it is found that the main controversial point is the time

365 of the first uplift of Bogda Mountain.

366 At present, there are many opinions about the time of the Bogda Mountain uplift. They think that the initial uplift of

367 Bogda Mountains occurred in Early Permian (Carroll et al., 1990; Shu et al., 2011; Wang et al., 2018; Li et al., 2022), Middle

368 Permian (Zhang et al., 2006; Liu et al., 2018; Wang et al., 2018), Late Permian-Early Triassic (Zhao et al., 2020; Guo et al.,

369 2006; Wang, 1996; Sun and Liu, 2009; Tang et al., 2014; Wang et al., 2018), Middle Triassic (Guo et al., 2006), Early Jurassic

370 (Green et al., 2005; Liu et al., 2017; Ji et al., 2018) and Late Jurassic (Yang et al., 2015). If the initial uplift of the Bogda

371 Mountains was after the middle Permian, the parent rock types of the Taodonggou Group mudstone in the Turpan-Hami Basin

372 and the Luchaogou Formation mudstone in the Junggar Basin should be the same.

373 We have counted the element geochemical characteristics of Luchaogou Formation in the Junggar Basin (Li et al., 2020)

374   and found that the parent rock type of Luchaogou Formation mudstone in the Junggar Basin is greatly different from that of

375   P_2td, which is felsic volcanic rock (Fig. 14). As a result, Bogda Mountain's initial uplift should be Late Permian-Early Triassic

376   in the Early Permian or Middle Permian. This is consistent with Li et al. (2022) and Wang et al. (2018), who inferred the uplift

377   of Bogda Mountain at 289.8 Ma–265.7 Ma. Shao et al. (2001) believed that the sandstone of the Daheyan Formation in

378   Turpan-Hami Basin has a good affinity with the Early Permian and Carboniferous, so the provenance direction of the

379   sandstone of the Daheyan Formation is consistent with that of the Early Permian, and they all come from the Jueluotage

380   Mountain. However, the paleocurrent direction of the Early Permian in Xinjiang is southeast (Zhang et al., 2005; Li et al.,

381   2007; Wang et al., 2019), and the provenance area is located in the north of the Bogda area. Zhao et al. (2020) calculated the

382   U-Pb dating results of 5250 zircons in the Tianshan and believed that the provenance of the Turpan-Hami Basin and the

383   Junggar Basin both came from the northern Tianshan and the Kelameili Mountain, which is also consistent with the ancient

384   ocean current direction in the Early Permian (Zhang et al., 2005; Li et al., 2007; Wang et al., 2019; Fig. 14a). Consequently,

385   the first uplift of Bogda Mountain should have occurred in the early Permian, but it was not exposed in the early Middle

386   Permian, and it still received sedimentation. In the middle Permian, the exposed water began to be denuded, becoming the

387   source area of the Turpan-Hami Basin (Wang et al., 2018).

388   Based on the above analysis, in the early Middle Permian, although Bogda Mountain in the north of Turpan-Hami Basin

389   was uplifted due to orogeny, it did not emerge from the water surface, and it still accepted the provenance of North Tianshan

390   and Kelameili Mountain. At this time, there was a NE-trending ancient ocean current (Carrollet et al., 1995; Obrist-Farnert et

391   al., 2015; Zhao et al., 2020), so Jueluotage Mountain, which has been uplifted in the south of Turpan-Hami Basin, became a

392   secondary provenance area (Shao et al., 1999; Fig. 14b). With the continuous uplift of Bogda Mountain, the sedimentary

393   center of Turpan-Hami Basin gradually shifted to Taibei Sag, and the provenance area of Turpan-Hami Basin changed to

394   Bogda Mountain and Jueluotage Mountain (Fig. 14c).

395   **5.3 sedimentation mode**

396   In previous studies, scholars have believed that the sedimentation of the Permian in the Turpan-Hami Basin is mainly

397   controlled by traction currents (Chen et al., 2003). However, recent research has revealed the presence of gravity flow deposits

398   in the Permian of the Turpan-Hami Basin (Wang et al., 2017; Wang et al., 2018; Xu, 2022). Yang et al. (2010) found poorly

399   sorted debris flow deposits in the Daheyan Formation, and Xu (2022) discovered alluvial and fluvial facies in the Daheyan

400   Formation, consisting of volcaniclastic rocks and conglomerates that are similar in composition to the Lower Permian

401   volcaniclastic rocks and conglomerates. This suggests the existence of gravity flow deposits during the early Permian in the

402   Turpan-Hami Basin. Wang et al. (2018) also suggested the development of gravity flow deposits and pillow lavas in the Early

403   Permian. Meanwhile, in the early Middle Permian, the sedimentation inherited the provenance and sedimentation style from

404   the early Permian, but the gravity flow deposits transitioned gradually into traction current deposits. Due to the influence of

gravity flow deposits, terrestrial organic matter can be transported to the deep lake area (Yu et al., 2022; Li et al., 2011), thereby altering the type of organic matter.

During the middle of the Taodonggou Group, the Turpan-Hami Basin entered the foreland basin sedimentation stage due to the uplift of the Bogda Mountains. The sedimentary environment of the Taodonggou Group in the Tainan Sag is similar to that in the Taibei Sag (Li, 2019). During this time, the sedimentary water body of the Taodonggou Group in the Turpan-Hami Basin became shallower, and the dominant sedimentation style transitioned to traction currents. Xu (2022) conducted lithological observations on the Taerlanggou section, the Zhaobishan section, and the Y well in the Taodonggou Group and found the presence of traction structures of gravity flow origin in the middle and upper parts of the Taerlang Formation. Additionally, a large number of calcareous and iron nodules appeared in the formation, indicating the occurrence of gravity flow deposits during the late-stage sedimentation of the Taodonggou Group. The organic matter type in the mudstones during this period was influenced by gravity flows.

5.4 Formation mechanism of the Taodonggou Group mudstone

Based on the sedimentary environment, provenance, and sedimentation mode during the deposition of the Taodonggou Group mudstones, this study has constructed the formation mechanism of the Taodonggou mudstones. The results indicate that the formation of the Taodonggou Group mudstones can be divided into three stages.

In the early of the Taodonggou Group, Bogda Mountain began to rise but did not emerge from the water surface. The sediment source is mainly from North Tianshan and Kelameili Mountain, and the secondary source area is Jueluotage Mountain in the south of the Turpan-Hami basin. The stratum of the Taodonggou Group was deposited in a warm and humid paleoclimate with high weathering intensity and a stable input of terrigenous detritus. In addition, the sedimentary water body is deep at this time, creating a deep lake environment of brackish water and dyoxic. However, this period inherited the gravity flow sedimentation characteristics from the Early Permian. Due to the influence of gravity flows, terrestrial organic matter was transported to the deep lake, resulting in the input of organic matter in the mudstones primarily derived from terrestrial higher plants (Miao et al., 2021). Consequently, a high-quality Type III organic matter source rock was formed (Fig.15a).

In the middle of the Taodonggou Group, with the continuous uplift of Bogda Mountain and hydrothermal activity, the climate changed into a hot and humid paleoclimate, the weathering degree further increased, and the input of terrigenous detritus increased. The provenance areas are Bogda Mountain and Jueluotage Mountain. In addition, during this period, the sedimentary center gradually transferred to the Taibei sag, and the sedimentary water body became shallow, which was a dyoxic intermediate-depth lake environment. Due to the nutrients brought by hydrothermal activities, the lower algae multiplied during this period, and the salinity of the sedimentary water body became lower, becoming a freshwater environment and thus depositing a set of high-quality II_2 organic source rocks.

In the late Taodonggou Group, the uplift of Bogda Mountain basically stopped, and the climate changed to a warm and humid paleoclimate again. The weathering degree was high, and the input of terrigenous debris was reduced. Bogda Mountain

and Jueluotage Mountain remained the provenance areas. The sedimentary center was essentially transferred to the Taibei Sag at this time. During this period, the salinity of the sedimentary water body was high, and the sedimentary water body became deeper. It was a deep lake environment with dyoxic and brackish water. During this period, the sedimentation was also influenced by gravity flows, leading to changes in lithology and organic matter type. As a result, the organic matter type in the mudstones deposited during this period transitioned to Type III.

6 Conclusion

Through the mineral composition and element geochemistry analysis of the Taodonggou Group mudstone, the following understandings have been obtained:

(1) The mudstone minerals of the Taodonggou Group are mainly clay and quartz and can be classified into 4 petrographic types according to their mineral fractions.

(2) The Taodonggou Group mudstone was deposited in an intermediate-depth or deep, dyoxic, freshwater-brackish lake environment under warm and humid paleoclimatic conditions. The input of terrestrial debris was stable, but the sedimentation rate was slow. In addition, the sedimentation in the middle stage was influenced by hydrothermal activities. In addition, the source rocks of the Taodonggou Group mudstone are mainly andesitic and feldspathic volcanic rocks. Sediment sorting and recycling were weak, and hydrocarbon source information was well preserved. The tectonic background of the source area was a continental island arc and an oceanic island arc.

(3) The sedimentary environment, sources, and sedimentary methods have significant impacts on the organic matter types of the Taodonggou Group. In the early taodonggou Group, the sedimentation center was in the Bogda area. At this time, the Bogda Mountain region was not exposed, and the depositional processes inherited the characteristics of Early Permian gravity flow sedimentation, resulting in the widespread deposition of a series of high-quality Type III source rocks in the basin. In the middle taodonggou Group, the sedimentation center gradually migrated to the Taibei Sag. During this period, the Bogda Mountain region experienced uplift and hydrothermal activity, and the depositional processes gradually transitioned to traction flows, resulting in the widespread deposition of a series of Type II source rocks in the basin. In the late taodonggou Group, the uplift of the Bogda Mountain region ceased, and the sedimentation center completely shifted to the Taibei Sag. Meanwhile, under the influence of gravity flows, the organic matter types of the Taodonggou mudstone changed to Type III.

Data availability

Data will be made available on request.

Acknowledgement

This study was supported by National Major Science and Technology Project of China (grant nos. 2016ZX05066001-002; 2017ZX05064-003-001; 2017ZX05035-02 and 2016ZX05034-001-05), Innovative Research Group Project of the National Natural Science Foundation of China (grant nos. 41872135 and 42072151), PetroChina Science and Technology

Project (grant nos. 2021DJ0602). We thank Hangzhou Yanqu Information Co., Ltd, Key Laboratory of natural gas accumulation, China National Petroleum Corporation and development and Beijing Orient Smart for providing testing samples and test equipments, as well as our colleagues' useful suggestions.

Author contribution

Miao H. and Guo J.Y. designed experiments, Wang Y.B. and Jiang Z.X. revised the first draft of the manuscript, Guo J. Y., Wang Y.B. and Jiang Z.X. provided financial support, Miao H. and Zhang C.J. provided language services and figure production, Li C.M. investigated and revised the ideas of the article, and Miao H. prepared the manuscript with your contributions. All authors contributed to the review of the manuscript.

Competing interests

The contact author has declared that none of the authors has any competing interests.

References

Algeo, T.J., and Ingall, E.: Sedimentary Corg:P ratios, paleocean ventilation, and Phanerozoic atmospheric pO2. Palaeogeogr. Palaeoclimatol. Palaeoecol., 256, 3–4, 130–155, 2007.

Algeo, T. J., and Maynard, J. B.: Trace-element behavior and redox facies in core shales of Upper Pennsylvanian Kansas-type cyclothems. Chem. Geol., 206, 3-4, 289-318, 2004.

Allègre, C. J., and Minster, J. F.: Quantitative models of trace element behavior in magmatic processes. Earth Planet. Sci. Lett., 38, 1–25, 1978.

Basu, A., Bickford, M. E., and Deasy, R.: Inferring tectonic provenance of siliciclastic rocks from their chemical compositions: A dissent. Sediment. Geol., 336, 26−35, 2016.

Bhatia, M. R.: Plate tectonics and geochemical composition of sandstones. J. Geol., 91, 611– 627, 1983.

Bhatia, M. R., and Crook, K. A. W.: Trace element characteristics of graywackes and tectonic setting discrimination of sedimentary basin. Contrib. Mineral. Petrol., 92, 181–193, 1986.

Cai, Y. L., Ouyang, F., Luo, X. R., Zhang, Z. L., Wen, M. L., Luo, X. N., and Tang, R.: Geochemical Characteristics and Constraints on Provenance, Tectonic Setting, and Paleoweathering of Middle Jurassic Zhiluo Formation Sandstones in the Northwest Ordos Basin, North-Central China. Minerals, 12,5, 603, 2022.

Cao, L., Zhang, Z. H., Zhao, J. Z., Jin, X., Li, H., Li, J. Y., and Wei, X. D.: Discussion on the applicability of Th/U ratio for evaluating the paleoredox conditions of lacustrine basins. Int. J. Coal geol., 248, 103868, 2021.

Cao, J., Yang, R. F., Yin, W., Hu, G., Bian, L. Z., and Fu, X. G.: Mechanism of Organic Matter Accumulation in Residual Bay Environments: The Early Cretaceous Qiangtang Basin, Tibet. Energy & Fuels, 32,2, 1024-1037, 2018.

Carroll, A., Graham, S., Hendrix, M., Ying, D., and Zhou, D.: Late Paleozoic tectonic amalgamation of northwestern China: sedimentary record of the northern Tarim, northwestern Turpan, and southern Junggar basins.Geol. Soc. Am. Bull., 107, 5,

499   571-594, 1995.

500   Carroll, A., Liang, Y. H., Graham, S., Xiao, X. H., Hendrix, S., Chu, J. C., and McKnight, L.: Junggar basin, northwest China:

501   trapped Late Paleozoic Ocean. Tectonophysics, 181, 1–14, 1990.

502   Chen. X., Niu, R.J., and Cheng, J.H.: The Sequence stratigraphy of Middle Permian-Triassic in Turpan-Hami Basin. Xinjiang

503   Pet. Geol., 24, 6, 494-497, 2003.

504   Deditius, A.: Arsenic Environmental Geochemistry, Mineralogy, and Microbiology. Reviews in Mineralogy and Geochemistry,

505   vol 79. Economic Geology, 110, 7, 1905-1907, 2015.

506   Essefi, E.: Geochemistry and mineralogy of the sebkha Oum El Khialate evaporites mixtures, southeastern Tunisia. Resource

507   Geology, 71, 3, 242-249, 2021.

508   Floyd, P. A., Leveridge, B. E.: Tectonic environment of the Devonian Gramscatho Basin, South cornwall: framework mode

509   and geochemical evidence from turibiditic sandstones. Journal of the Geological Society, 144, 4, 531-542, 1987.

510   Gehrels, G. E., Valencia, V. A., and Ruiz, J.: Enhanced precision, accuracy,efficiency, and spatial resolution of U-Pb ages by

511   laser ablation-multicollector-inductively coupled plasma-massspectrometry. Geochem., Geophys., Geosyst., 9, 3, 1– 13, 2008.

512   Glaser, K. S., Miller, C. K., Johnson, G. M., Kleinberg, R. L., and Pennington, W. D.: Seeking the sweet spot: Reservoir and

513   completion quality in organic shales. Oilfield Review, 25, 16–29, 2014.

514   Greene, T. J., Carroll, A. R., Wartes, M., Graham, S. A., and Wooden, J. L.: Integrated provenance analysis of a complex

515   orogenic terrane: Mesozoic uplift of the Bogda Shan and inception of the Turpan-Hami Basin, NW China. Journal of

516   Sedimentary Research, 75, 20, 251-267, 2005.

517   Guo, Z., Zhang, Z., Wu, C., Fang, S., and Zhang, R.: The Mesozoic and Cenozoic exhumation history of Tianshan and

518   comparative studies to the junggar and Altai mountains Acta Geol. Sin.: 80, 1, 1-15, 2006.

519   Hatch, J.R., and Leventhal, J.S.: Relationship between inferred redox potential of the depositional environment and

520   geochemistry of the Upper Pennsylvanian (Missourian) Stark shale member of the Dennis Limestone, Wabaunsee County,

521   Kansas, USA. Chem. Geol., 99, 65–82, 1992.

522   Herkat, M., and Ladjal, A.: Paleobathymetry of foraminiferal assemblages from the Pliocene of the Western Sahel (North-

523   Algeria). Palaeogeography Palaeoclimatology 374, 144-163, 2013.

524   Hu, F., Meng, Q., and Liu, Z.: Mineralogy and element geochemistry of oil shales in the Lower Cretaceous Qingshankou

525   Formation of the southern Songliao Basin, northeast China: implications of provenance, tectonic setting, and

526   paleoenvironment. ACS Earth Space Chem., 5, 365−380, 2021.

527   Ji, H., Tao, H., Wang, Q., Qiu, Z., Ma, D., Qiu, J., and Liao P.: Early to middle Jurassic tectonic evolution of the Bogda

528   mountains, northwest China: evidence from sedimentology and detrital zircon geochronology. J. Asian Earth Sci., 153, 57-74,

529   2018.

Jiang, S. H., Li, S. Z., Somerville, I. D., Lei, J. P, and Yang, H. Y.: Carboniferous-Permian tectonic evolution and sedimentation of the Turpan-Hami Basin, NW China: Implications for the closure of the Paleo-Asian Ocean. J. Asian Earth Sci., 113, 644-655, 2015.

Kidder, D. L., and Erwin, D. H.: Secular distribution of biogenic silica through the phanerozoic: Comparison of silica-replaced fossils and bedded cherts at the series level. J. GEOL., 109, 4, 509-522, 2001.

Korobkin, V. V., and Buslov, M. M.: Tectonics and geodynamics of the western Central Asian Fold Belt (Kazakhstan Paleozoides). Russian Geology and Geophysics, 52, 12, 1600-1618, 2011.

Kröner, S. R., and McLennan, S. M.: The Continental Crust: Its Composition and Evolution; Blackwell: Oxford, 312,1985.

Kroonenberg, S.B.: Effect of provenance, sorting and weathering on the geochemistry of fluvial sands from different tectonic and climatic environments. In Proceedings of the 29th International Geological Congress, Part A, Kyoto, Japan, 24 August– 3 September, 69, 81, 1992.

Lerman, A., and Baccini, P.: Lakes: Chemisty, Geology, Physics. Springer-Verlag, New York, 1978.

Li, C. M., Liu, J. T., Ni, L. B., and Fan, S. W.: Characteristics of deep geological structure and petroleum exploration prospect in Turpan-Hami Basin. China Petroleum Exploration, 26, 4, 44-57, 2021. (In Chinese with English abstract)

Li, L., Qu, Y.Q., Meng, Q.R., and Wu, G.L.: Gravity Flow Sedimentation: Theoretical Studies and Field Identification. Acta Sedimentologica Sinica, 29,4, 677-688, 2011.

Li, RB.: Filling characteristic and research significance of Permian in Tainan Depression of Tuha Basin. J. Jilin Universitry (Earth science Edition) 49, 6, 1518-1528, 2019.

Li, Y. J., Sun, P. C., Liu, Z. J., Yao, S. Q., Xu, Y. B., and Liu, R.: Geochemistry of the Permian Oil Shale in the Northern Bogda Mountain, Junggar Basin, Northwest China: Implications for Weathering, Provenance, and Tectonic Setting. ACS Earth and Space Chemistry4, 8, 1332-1348, 2020.

Li, Y. L., Shan, X., Gelwick, K. D., Yu, X. H., Jin, L. N., Yao, Z. Q., Li, S. L., and Yang, S. Y.: Permian mountain building in the bogda mountains of NW China. International Geology Review, 2048270, 2022.

Li, W., Hu, J., Li, D., Liu, J., Sun, Y., and Liang, J.: Analysis of the late Paleozoic and Mesozoic paleocurrents and It's constructional significance of the northern Bogdashan, Xinjiang. Acta Sedimentol. Sin., 25,2, 283-292, 2007.

Liu, D., Zhang, C., Yao, E., Song, Y., Jiang, Z., and Luo, Q.: What generated the Late Permian to Triassic unconformities in the southern Junggar Basin and western Turpan Basin; tectonic uplift, or increasing aridity? Palaeogeogr. Palaeoclimatol. Palaeoecol., 468, 1-17, 2017.

Liu, D., Kong, X., Zhang, C., Wang, J., Yang, D., Liu, X., Wang, X., and Song, Y.: Provenance and geochemistry of Lower to Middle Permian strata in the southern Junggar and Turpan basins: a terrestrial record from mid-latitude NE Pangea. Palaeogeogr. Palaeoclimatol. Palaeoecol., 495, 259-277, 2018.

Liu, G., Zhou, D.: Application of microelements analysis in identifying sedimentary environment-taking Qianjiang Formation in the Jiang Han Basin as a example. Pet. Geo. Exp. 29,3, 307-311,2007. (In Chinese with English abstract)

Maravelis, A. G., Offler, R., Pantopoulos, G., and Collins, W. J.: Provenance and tectonic setting of the Early Permian sedimentary succession in the southern edge of the Sydney Basin, eastern Australia. Geological J. 56, 4, 2258-2276, 2021.

McLennan, S. M., Hemming, S., McDaniel, D. K., and Hanson, G.N.: Geochemical approaches to sedimentation, provenance, and tectonics. Spec. Pap. Geol. Soc. Am. 284, 21−40, 1993.

McLennan, S. M., Taylor, S. R., and Kröner, A.: Geochemical evolution of Archean shales from South Africa I: The Swaziland and Ponggola Supergroups. Precambrian Res., 22, 93– 124, 1983.

Mei, X., Li, X.J., Mi, P.P., Zhao, L., Wang, Z.B., Zhong, H.X., Yang, H., Huang, X.T, He, M.Y., Xiong, W., and Zhang, Y.: Distribution regularity and sedimentary differentiation patterns of China seas surface sediments. Geology in China, 47,5,1447-1462, 2020. (In Chinese with English abstract)

Miao, H., Wang, Y. B., Guo, J. Y., Fu, Y., and Li, J. H.: Weathering correction and hydrocarbon generation and expulsion potential of Taodonggou Group source rocks in Taibei Sag in Turpan-Hami Basin. Petroleum Geology & Oilfield Development in Daqing, 42,2, 22-32, 2023.

Miao, H., Wang, Y. B., Guo, J. Y., Han, W. L., and Gong, X.: Evaluation of Middle Permian source rocks of the Taodonggou Group in the Turpan Hami Basin. Geophysical Prospecting for Petroleum, 61, 4, 733-742, 2022. (In Chinese with English abstract)

Miao, H., Wang, Y. B., He, C., Li, J. H., Zhang, W., Zhang, Y. J., and Gong, X.: Fault development characteristics and reservoir control in Chengbei fault step zone,Bohai Bay Basin. Lithologic Reservoirs, 34, 2, 105-115, 2022a. (In Chinese with an English abstract).

Miao, H., Wang, Y. B., Ma, Z. T., Guo, J. Y., and Zhang, Y. J.: Generalized Deltalog R model with spontaneous potential and its application in predicting total organ carbon content. Journal of Mining Science and Technology, 7, 4, 417-426, 2022b. (In Chinese with English abstract)

Miao, H., Wang, Y. B., Zhao, S. H., Guo, J. Y., Ni, X. M., Gong, X, Zhang, Y. J., and Li, J. H.: Geochemistry and Organic Petrology of Middle Per-mian Source Rocks in Taibei Sag, Turpan-Hami Basin, China: Implication for Organic Matter Enrichment. ACS Omega, 6,47, 31578-31594, 2021.

Miao, J. Y., Zhou, L. F., Deng, K., Li, J. F., Han, Z. Y., and Bu, Z. Q.: Organic Matters from Middle Permain Source rocks of Northern Xinjiang and Their Relationships with Sedimentary environments. Geochemica, 6,551-560, 2004. (In Chinese with English abstract)

Nesbitt, H. W., and Young, G. M.: Prediction of some weathering trends of plutonic and volcanic rocks based on thermodynamic and kinetic considerations. Geochim. Cosmochim. Acta., 48, 7, 1523-1534, 1984.

Novikov, I. S.: Reconstructing the stages of orogeny around the Junggar basin from the lithostratigraphy of Late Paleozoic, Mesozoic, and Cenozoic sediments. Russian Geology and Geophysics. 54, 2, 138-152, 2013.

Obrist-Farner, J., Yang, W., and Hu, X. F.: Nonmarine time-stratigraphy in a rift setting: an example from the Mid-Permian lower Quanzijie low-order cycle Bogda Mountains, NW China. J. Palaeogeogr., 4, 1, 27-51, 2015.

Pinto, L., Munoz, C., Nalpas, T., and Charrier, R.: Role of sedimentation during basin inversion in analogue modelling. Journal of Structural Geology, 32, 4, 554-565, 2010.

Rollinson, H. R.: Using Geochemical Data: Evaluation, Presentation, Interpretation; Longman Scientific Technical: New York, 1993.

Rosenthal, Y., Lam, P., Boyle, E. A., and Thomson, J.: Authigenic cadmium enrichments in suboxic sediments: precipitation and postdepositional mobility - sciencedirect. Earth & Planetary Science Letters, 132, 1-4, 99-111, 1995.

Roser, B. P., Korsch, R. J.: Provenance Signatures of Sandstone-mudstone suites determined using discriminant functiom analysis of major-element data. Chem. Geol. 67, 119– 139, 1988.

Ross, D.J.K., and Bustin, R. M.: Investigating the use of sedimentary geochemical proxies for paleoenvironment interpretation of thermally mature organic-rich strata: Examples from the Devonian–Mississippian shales, Western Canadian Sedimentary Basin. Chem. Geol., 260, 1–19, 2009

Schoepfer, S. D., Shen, J., Wei, H. Y., Tyson, R. V., Ingall, E., and Algeo, T. J.: Total organic carbon, organic phosphorus, and biogenic barium fluxes as proxies for paleomarine productivity. Earth Sci. Rev., 149, 23–52, 2015.

Shao, L., Li, W.H., and Yuan, M.S.: Characteristic of sandstone and its tectonic implications of the Turpan Basin. Acta Sedimentologica Sinica, 17,3, 435–441, 1999.

Shao, L., Stattegger, K., and Garbe-Schoenberg, C.: Sandstone petrology and geochemistry of the Turpan Basin (NW China): implications for the tectonic evolution of a Continental Basin. Journal of Sedimentary Research, 71, 1, 37–49,2001. (In Chinese with English abstract)

Shi, J., Zou, Y. R., Cai, Y. L., Zhan, Z. W., Sun, J. N., Liang, T., and Peng, P. A.: Organic matter enrichment of the Chang 7 member in the Ordos Basin: Insights from chemometrics and element geochemistry. Marine Petroleum Geology, 134, 105306, 2021.

Shi, Y. Q, Ji, H. C., Yu, J. W, Xiang, P. F., Yang, Z. B, and Liu, D. D.: Provenance and sedimentary evolution from the Middle Permian to Early Triassic around the Bogda Mountain, NW China: A tectonic inversion responding to the consolidation of Pangea. Mar. Pet. Geol., 114, 104169, 2020.

Shu, L., Wang, B., Zhu, W., Guo, Z., Charvet, J., and Zhang, Y.: Timing of initiation of extension in the Tianshan, based on structural, geochemical and geochronological analyses of bimodal volcanism and olistostrome in the Bogda Shan (NW China). Int. J. Earth Sci., 100, 7, 1647-1663, 2011.

Song, J., Bao, Z., Zhao, X. M., Gao, Y. S., Song, X. M., Zhu, Y. Z., Deng, J., Liu, W., Wang, Z. C., Ming, C. D., Meng, Q. K., Zhang, L., Mao, S. W., Zhang, Y. L., Yu, X., and Wei, M. Y.: Sedimentology and geochemistry of Middle–Upper Permian in northwestern Turpan–Hami Basin, China: Implication for depositional environments and petroleum geology. Energy Exploration & Exploitation 36, 4, 910-941, 2018.

Sun, G., and Liu, Y.: The preliminary analysis of the uplift time of Bogda Mountain, Xinjiang, Northwest China. Acta Sedimentol. Sin., 27, 3, 487-491, 2009.

Tang, W., Zhang, Z., Li, J., Li, K., Chen, Y., and Guo, Z.: Late Paleozoic to Jurassic tectonic evolution of the Bogda area (northwest China): evidence from detrital zircon U–Pb geochronology. Tectonophysics, 626, 144-156, 2014.

Taylor, S. R., and Mclennan, S. M.: The continental crust: Its composition and evolution. Blackwell Science Publications, Oxford. 1985.

Thorpe, C. L., Law, G. T. W., Boothman, C., Lloyd, J. R., Burke, I. T., and Morris, K.: The Synergistic Effects of High Nitrate Concentrations on Sediment Bioreduction. Geomicrobiol. J., 29, 5, 484-493, 2012.

Tian, J.Q., Liu, J.Z., Zhang, Z.B., and Cong, F.Y.: Hydrocarbon-generating potential, depositional environments, and organisms of the Middle Permian Tarlong Formation in the Turpan-Hami Basin, northwestern China. GSA Bulletin 129, 9-10, 1252–1265, 2017.

Tribovillard, N., Algeo, T. J., Baudin, F., and Riboulleau, A.: Analysis of marine environmental conditions based on molybdenum–uranium covariation—applications to Mesozoic paleoceanography. Chem. Geol. 324,46–58, 2012.

Tribovillard, N., Algeo, T. J., Lyons, T., and Riboulleau, A.: Trace metals as paleoredox and paleoproductivity proxies: an update. Chemical Geology 232, 1–2, 12–32, 2006.

Trbovillard, N. P., Desprairies, A., Lallier-verges, E., Bertrand, P., Moureau, N., Ramdani, A., and Ramanampiso, L.: Geochemical study of organic-matter rich cycles from the Kimmeridge Clay Formation of Yorkshire (UK): productivity versus anoxia. Palaeogeography, Palaeoclimatology, Palaeoecology, 108,1-2,165-181, 1994.

Wartes, M. A., Carroll, A. R., and Greene, T. J.: Permian sedimentary record of the Turpan-Hami basin and adjacent regions, northwest China: Constraints on postamalgamation tectonic evolution. Geological Society of America Bulletin, 114,2, 131-152, 2002.

Wang, A., Wang, Z., Liu, J., Xu, N., Li, H.: The Sr/Ba ratio response to salinity in clastic sediments of the Yangtze River Delta. Chem. Geol., 559, 119923, 2021.

Wang, L.: Sediment flux and mechanism for the uplifting of the mountain system around the Junggar inland basin Sediment. Geol. Tethyan Geol., 16, 3, 39-46, 1996.

Wang, J., Cao, Y. C., Wang, X. T., Liu, K. Y., Wang, Z. K., and Xu, Q. S.: Sedimentological constraints on the initial uplift of the West Bogda Mountains in Mid-Permian. Sci. Rep. 8, 1453, 2018.

Wang, J., Wu, C., Li, Z., Zhu, W., Zhou, T., Wu, J., and Wang, J.: The tectonic evolution of the Bogda region from Late Carboniferous to Triassic time: evidence from detrital zircon U–Pb geochronology and sandstone petrography. Geol. Mag., 155, 5, 1063-1088, 2018.

Wang, J., Wu, C., Zhou, T., Zhu, W., Zhou, Y., Jiang, X., and Yang, D.: Source-to-Sink analysis of a transtensional rift Basin from syn-rift to uplift stages. J. Sediment. Res. 89, 4, 335-352, 2019.

Wang, J. L., Wu, C. D., Zhou, T. Q., Zhu, W., Li, X. Y., and Zhang, T.: Source and sink evolution of a Permian–Triassic rift–drift basin in the southern Central Asian Orogenic Belt: Perspectives on sedimentary geochemistry and heavy mineral analysis. Journal of Asian Earth Sciences 181, 103905, 2019.

Wang, Y.: Mixed Sedimentary Characteristics and Pattern of the Fan Delta in the Middle Permian Taerlanggou Profile,Xinjiang Province Acta Sedimentologica Sinica, 37, 5, 922-933, 2019. (In Chinese with English abstract)

Wang, Z. W., Yu, F., Wang, J., Fu, X. G., Chen, W. B., Zeng, S. Q., and Song, C. Y.: Palaeoenvironment evolution and organic matter accumulation of the Upper Triassic mudstone from the eastern Qiangtang Basin (Tibet), eastern Tethys. Marine and Petroleum Geology 130, 105113, 2021.

Wronkiewicz, D. J., and Condie, K. C.: Geochemistry of archean shales from the witwatersrand supergroup, south Africa: Source-area weathering and provenance. Geochimica Cosmochimica Acta 51, 9, 2401-2416, 1987.

Wei, H., Chen, D. Z., Wang, J. G., Yu, H., and Tucker, M. E.: Organic accumulation in the lower Chihsia Formation (Middle Permian) of South China: Constraints from pyrite morphology and multiple geochemical proxies. Palaeogeogr. Palaeoclimatol. Palaeoecol., 353, 73-86, 2012.

Wei, X.X.: Middle-Late Permian fossil woods from Northern Tuha Basin: Implications for Palaeoclimate. MS thesis, Wuhan: China university of Geosciences, 2015. (In Chinese with English abstract)

Wu, C., Li, H. W., Sheng, S. Z., Chen, T., Shi, X. F., and Jiang, M. L.: Characteristics and main controlling factors of hydrocarbon accumulation of Permian-Triassic in Lukeqin structural zone, Tuha Basin. China Petroleum Exploration 26, 4, 137-148, 2021. (In Chinese with English abstract)

Xiong, X. H., and Xiao, J. F.: Geochemical Indicators of Sedimentary Environments—A Summary. Earth and Environment 39, 3, 405-414, 2011. (In Chinese with English abstract)

Xu, C., Shan, X. L., Lin, H. M., Hao, G. L., Liu, P., Wang, X. D., Shen, M. R., Rexiti, Y., Li, K., Li, Z. S., Wang, X. M., Du, X. D., Zhang, Z.W., Jia, P. M., and He, W. T.: The formation of early Eocene organic-rich mudstone in the western Pearl River Mouth Basin, South China: Insight from paleoclimate and hydrothermal activity. International Journal of Coal geology 253, 103957, 2022.

Xu, H.Y.: Characteristics of Permian Dark Fine-Grained Sedimentary rocks and their shale oil and gas Sigificance in the Northern Margin of Turpan-Hami Basin. MS thesis, Xi'an: Chang'an University, 2022. (In Chinese with English abstract)

Yang, Y., Song, C., and He, S.: Jurassic tectonostratigraphic evolution of the Junggar basin, NW China: a record of Mesozoic intraplate deformation in Central Asia. Tectonics 34, 1, 86-115, 2015.

Yang, W., Feng, Q., Liu, Y.Q., Tabor, N., Miggins, D., Crowley, J.L., Lin, J.Y., and Thomas, S.: Depositional environments and cyclo- and chronostratigraphy of uppermost Carboniferous–Lower Triassic fluvial–lacustrine deposits, southern Bogda Mountains, NW China — A terrestrial paleoclimatic record of mid-latitude NE Pangea. Global and Planetary Change, 73, 2010, 15-113, 2010.

You, J., Liu, Y., Zhou, D., Zheng, Q., Vasichenko, K., and Chen, Z.: Activity of hydrothermal fluid at the bottom of a lake and its influence on the development of high-quality source rocks: Triassic Yanchang Formation, southern Ordos Basin, China. Australian Journal of Earth Sciences 67, 1, 115-128, 2019.

Yu, Y., Cai, H.L., Yin, T.J., Zhang, X.Q., Xu, H., Huang, Y.R., and Cao, T.T.: Sedimentary Characteristics and Depositional Model of Lacustrine Gravity Flow Deposits: A case study of the Cretaceous Pointe Indienne Formation of Block A, Lower Congo Basin. Acta Sedimentologica Sinica, 2022, 40, 1, 34-46, 2022.

Zhang, C., He, D., Wu, X., Shi, X., Luo, J., Wang, B., Yang, G, Guan, S., and Zhao, X.: Formation and evolution of multicycle superimposed basins in Junggar Basin. China Petrol. Exp., 11, 1, 47-58, 2006.

Zhang, K., Song, Y., Jiang, S., Jiang, Z. X., Jia, C. Z., Huang, Y. Z., Wen, M., Liu, W. W., Xie, X. L., Liu, T. L., Wang, P. F., Shan, C. A., and Wu, Y. H.: Mechanism analysis of organic matter enrichment in different sedimentary backgrounds: A case study of the Lower Cambrian and the Upper Ordovician-Lower Silurian, in Yangtze region. Mar. Petrol. Geol., 99, 488–497, 2019.

Zhang, S., Liu, C., Bai, J., Wang, J., Ma, M., Guan, Y., and Peng, H.: Provenance variability of the Triassic strata in the Turpan-Hami basin: detrital zircon record of Indosinian tectonic reactivation in eastern Tianshan. Acta Geol. Sin. 93, 6, 1850-1868, 2019.

Zhang, S. C., Zhang, B. M., Bian, L. C., Jing, Z. J., Wang, D. R., Zhang, X. Y., Gao, Z. Y., and Chen, J. F.: Development constraints of marine source rocks in China. Earth Sci. Frontiers 12, 3, 39-48, 2005. (In Chinese with English abstract)

Zhao, R., Zhang, J. Y., Zhou, C. M., Zhang, Z. J., Chen, S., Stockli, D.F., Olariu, C., Steel, R., and Wang, H.: Tectonic evolution of Tianshan-Bogda-Kelameili mountains, clastic wedge basin infill and chronostratigraphic divisions in the source-to-sink systems of Permian-Jurassic, southern Junggar Basin. Mar. Petrol. Geol. 114, 104200, 2020.

Zhao, B. S., Li, R. X., Qin, X. L., Wang, N., Zhou, W., Khaled, A., Zhao, D., Zhang, Y. N., Wu, X. L., and Liu, Q.: Geochemical characteristics and mechanism of organic matter accumulation of marine-continental transitional shale of the lower permian Shanxi Formation, southeastern Ordos Basin, north China. Journal of Petroleum Science and Engineering, 205, 108815, 2021.

Zhu, Q. M., Lu, L. F., Pan A. Y.,Tao, J. Y., Ding, J. H., Liu, W. L., and Li, M. W.: Sedimentary environment and organic

716   matter enrichment of the Lower Cambrian Niutitang Formation shale, western Hunan Province, China. Petroleum Geology

717   & Experiment 43, 5, 797-854, 2021. (In Chinese with English abstract)

718   Zhu, X., Wang, B, Chen, Y., and Liu, H. S.: Constraining the Intracontinental Tectonics of the SW Central Asian Orogenic

719   Belt by the Early Permian Paleomagnetic Pole for the Turfan-Hami Block. Journal of Geophysical Research-solid earth, 124,

720   12, 12366-12387, 2019.
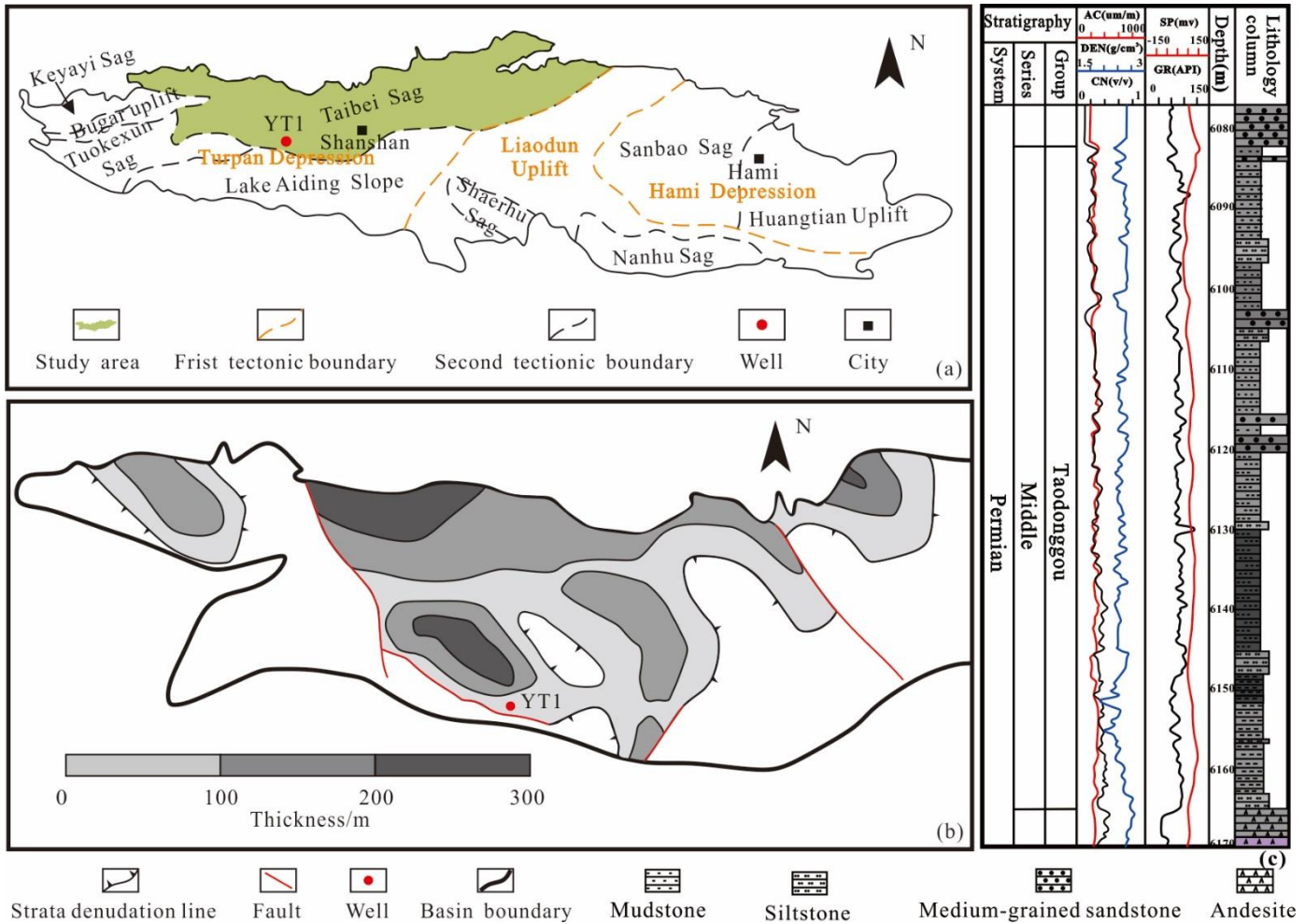
721

Figure1: Geological overview of the study area (modified after Miao et al., 2021; Miao et al., 2023): (a) Geological background of Turpan-

723 **Hami basin; (b) Thickness contour map of Taodonggou Group mudstone in Taibei sag; (c) YT1 stratum of Taodonggou Group**

724
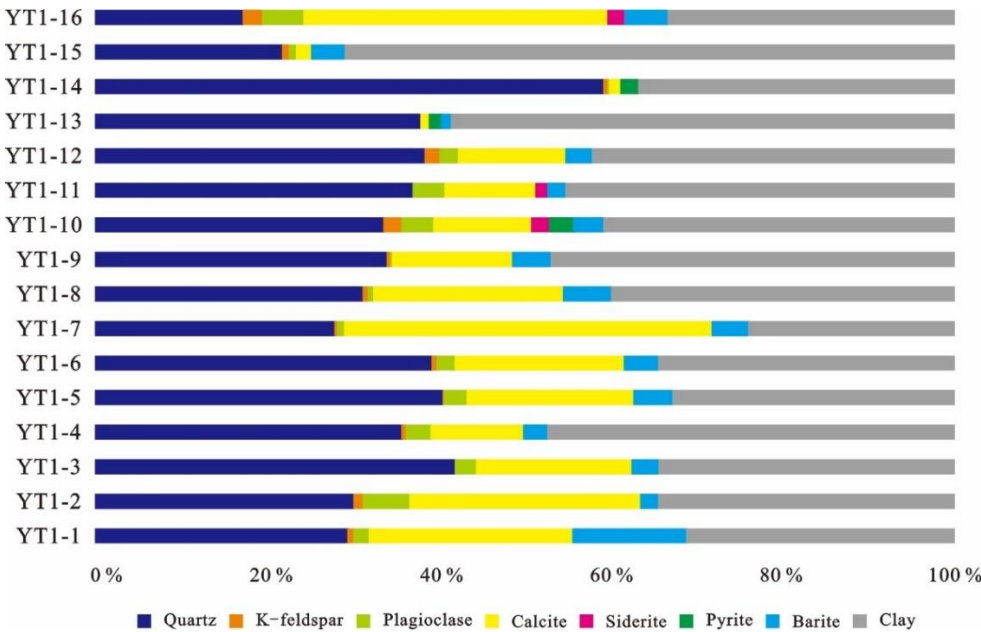
725 **Figure 2: Mineral composition of Taodonggou group mudstone in YT1 well**
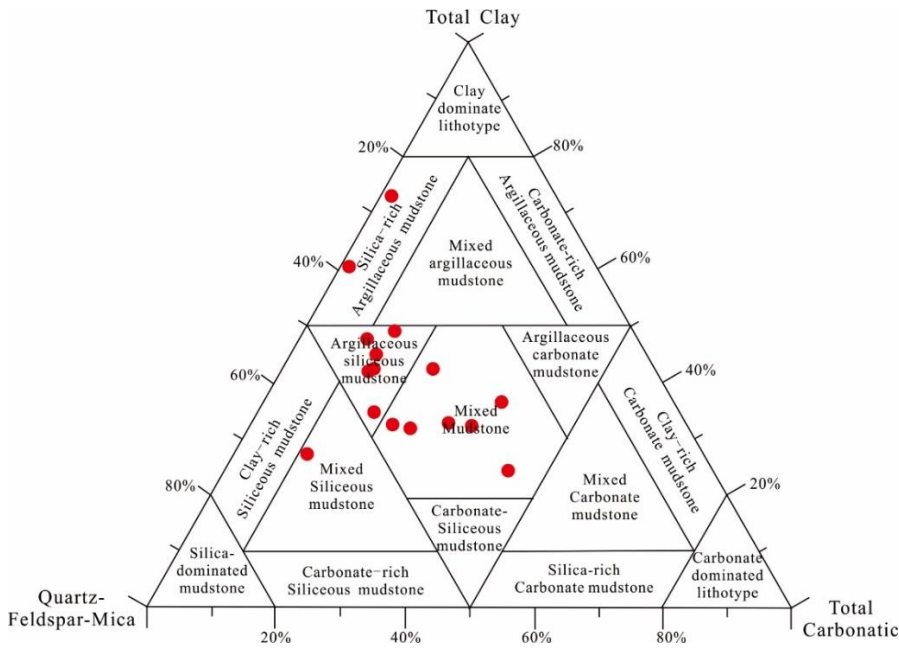
Figure 3: Lithofacies classification of Taodonggou Group mudstone in well YT1(modified from Glaser et al., 2014)
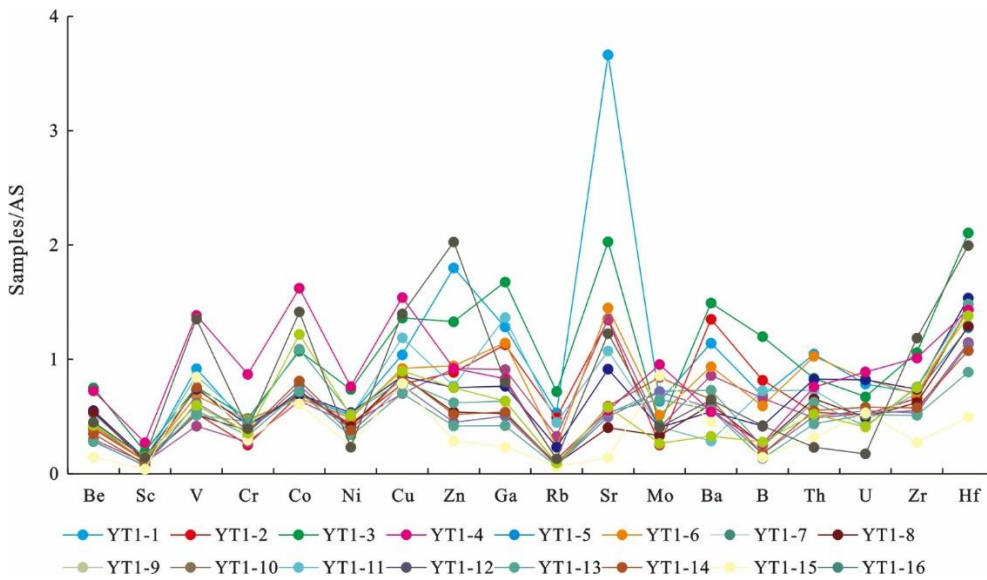
Figure 4: AS standardized multi-element diagrams of Taodonggou Group mudstone in the study area.
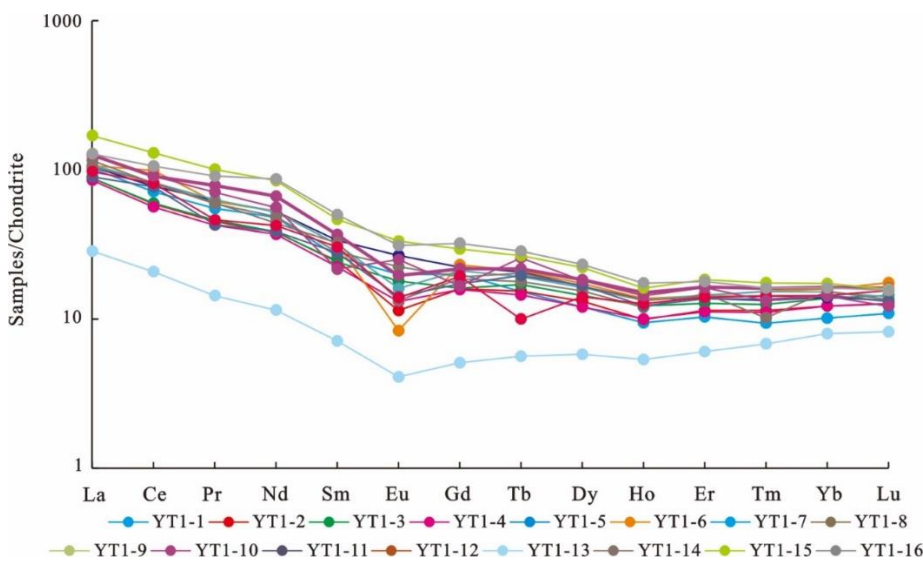
Figure 5: Standardized map of rare-earth element chondrite in mudstone of Taodonggou Group
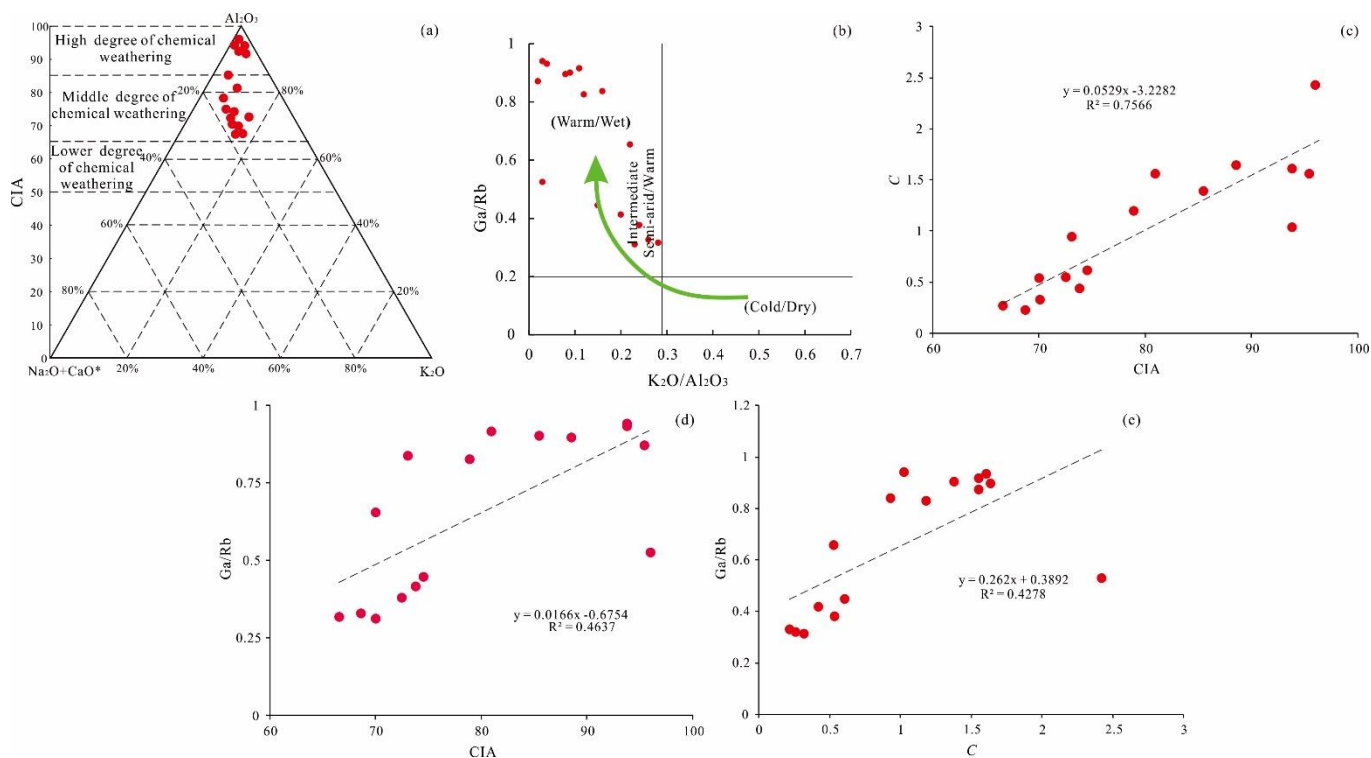
Figure 6: Paleoclimate of Taodonggou Group: (a) CIA Characteristics of Taodonggou Group mudstone (modified from Nesbitt and Young, 1984); (b) cross plot of K₂O/Al₂O₃ and Ga/Rb (modified from Roy and Roser, 2013); (c) cross plot of CIA and *C*; (d) cross plot of CIA and Ga/Rb; (e)cross plot of *C* and Ga/Rb
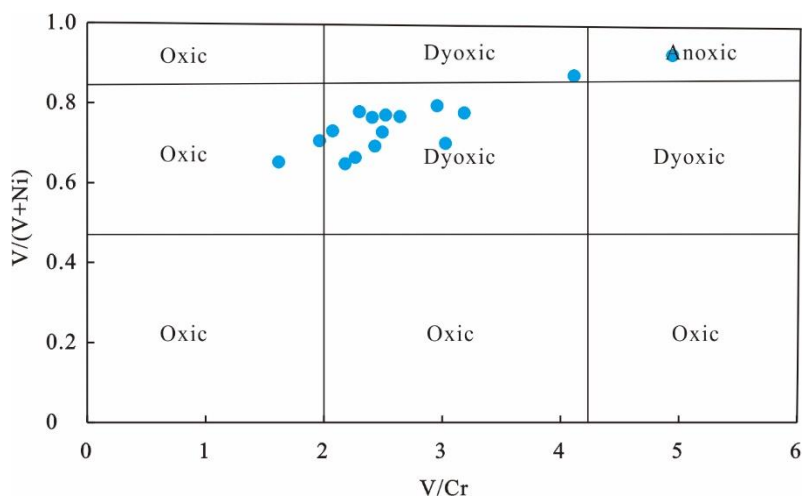
Figure7: Cross plot of V/Cr and V/(V+Ni)
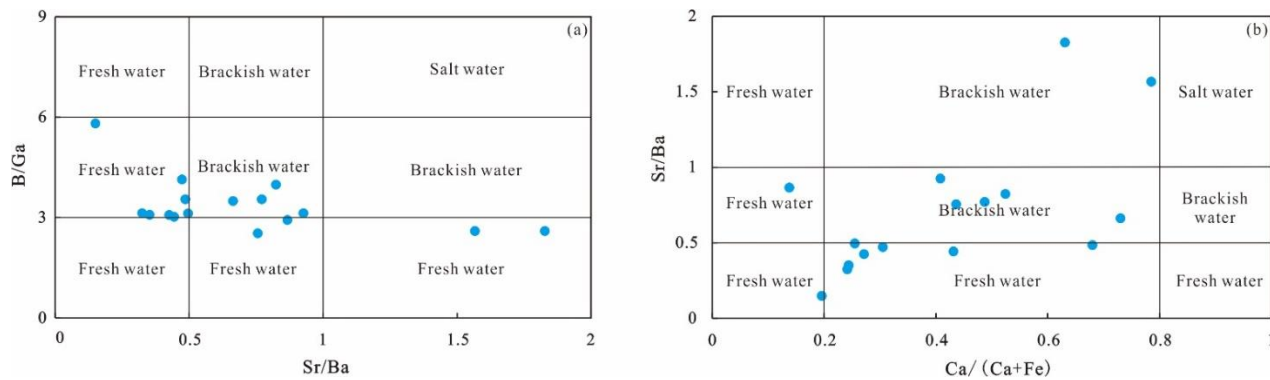
Figure 8: Cross plot of B/Ga and Sr/Ba (a) and cross plot of Ca/(Ca+Fe) and Sr/Ba (b)
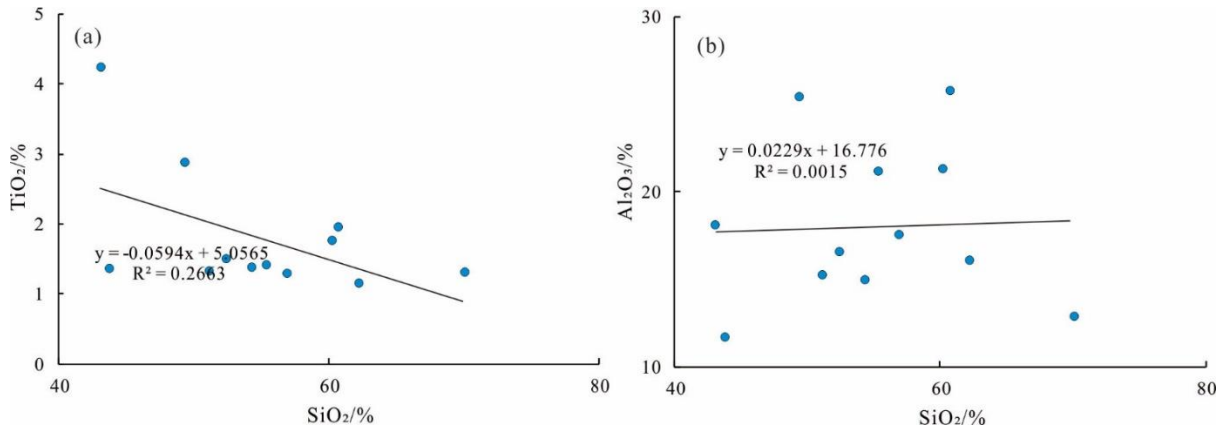
Figure 9: Intersection diagram of TiO$_2$ and SiO$_2$ (a) and intersection diagram of Al$_2$O$_3$ and SiO$_2$ (b)
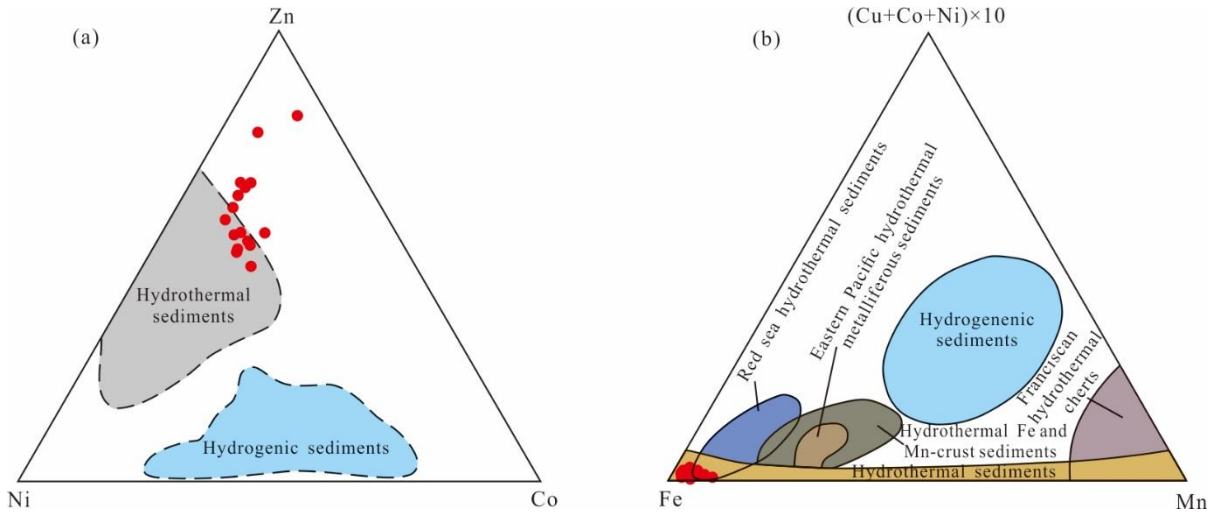
Figure 10: Zn-Ni-Co ternary diagram (a) and (Cu+Co+Ni) ×10-Fe-Mn ternary diagram (b) (modified after You et al., 2019)
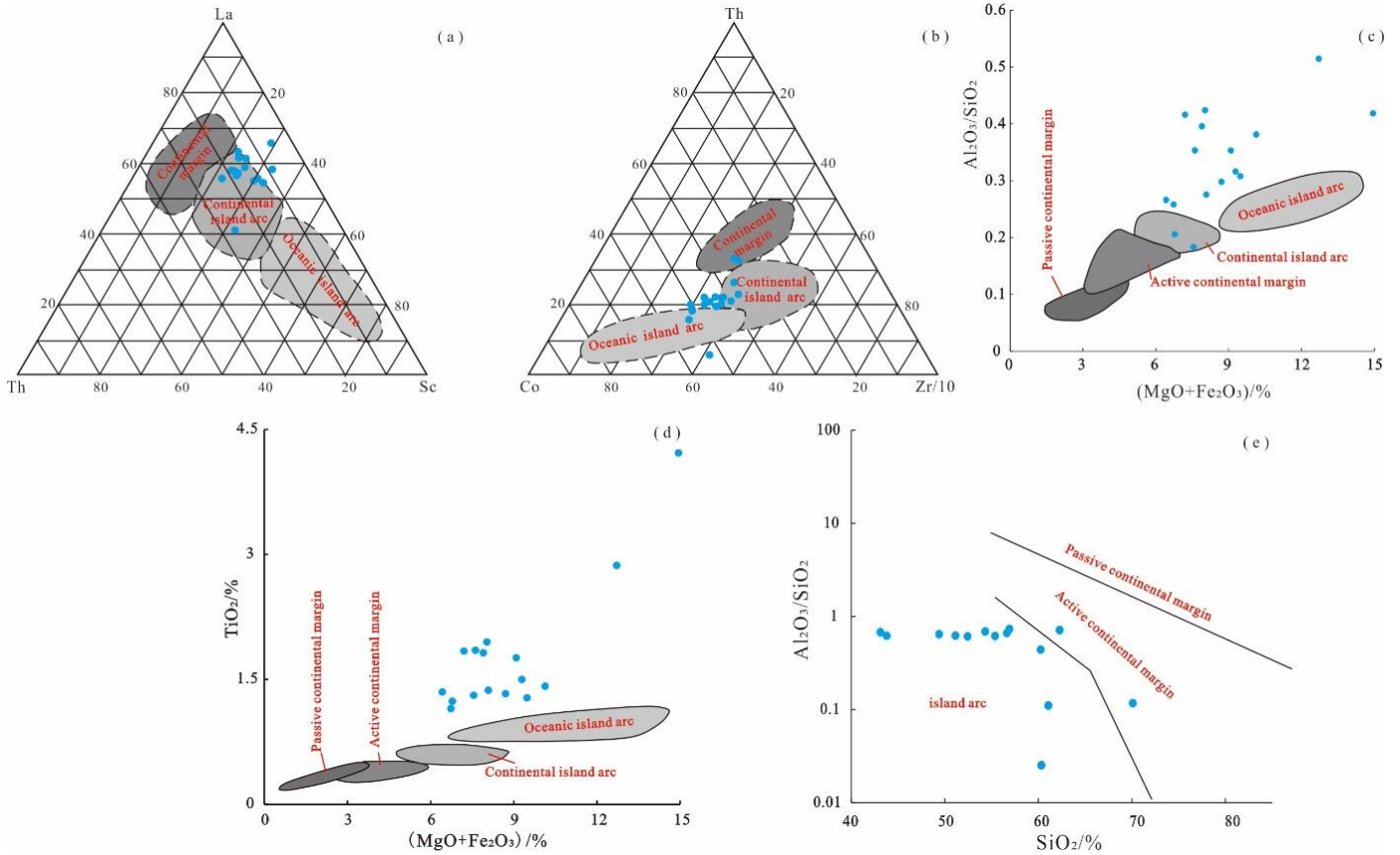
 Figure 11: Tectonic setting of source area in Taodonggou Group mudstone: (a) La-Th-Sc ternary diagram (modified after Zhu et al., 2021);

746 **(b) Th-Co-Zr/10 ternary diagram (modified after Zhu et al., 2021); (c) cross plot of Al₂O₃/SiO₂ and Fe₂O₃+MgO (modified after Bhatia,**

747 **1983); (d) cross plot of TiO₂ and Fe₂O₃+MgO (modified after Bhatia, 1983); (e) cross plot of SiO₂ and Al₂O₃/SiO₂ (modified after Roser**

748 **and Korsch, 1988)**
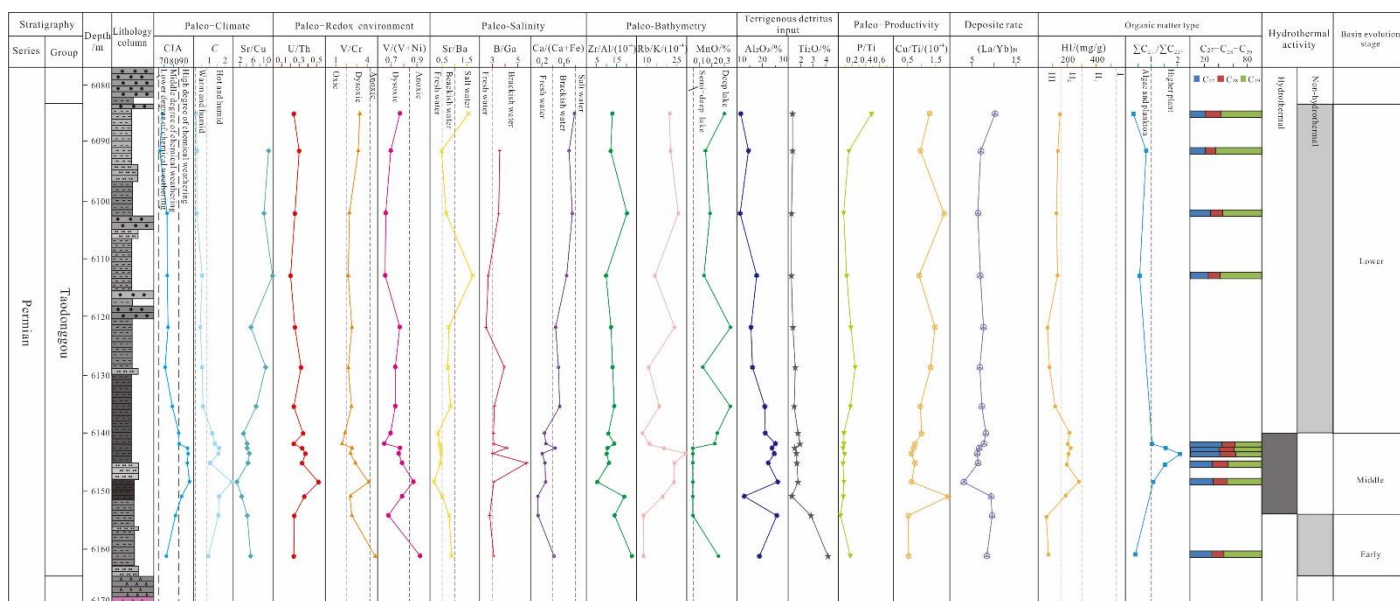
749

750 **Figure 12: The geochemical profile of the Taodonggou Group in YT1 well**
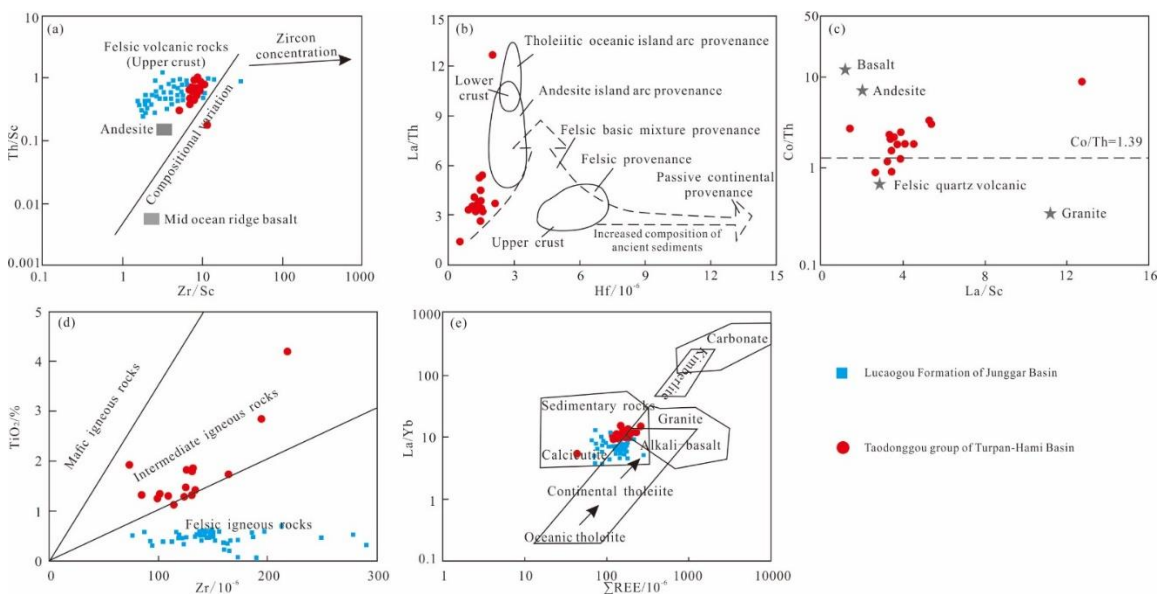
751

752 **Figure 13: Parent rock type of Taodonggou Group in YT1 well (Data of Lucaogou Formation in Junggar Basin are from Li et al., 2020):**

753 **(a) Th/Sc and Zr/Sc intersection diagram(modified after Floyd and Leveridge, 1987); (b) La/Th and Hf intersection diagram(modified**

754 **after Floyd and Leveridge, 1987); (c) Co/Th and La/Sc intersection diagram(modified after Wronkiewicz and Condie, 1987); (d) TiO₂ and**

755 **Zr intersection diagram; (e) La/Yb and ∑REE intersection diagram (modified after Allègre and Minster, 1978)**
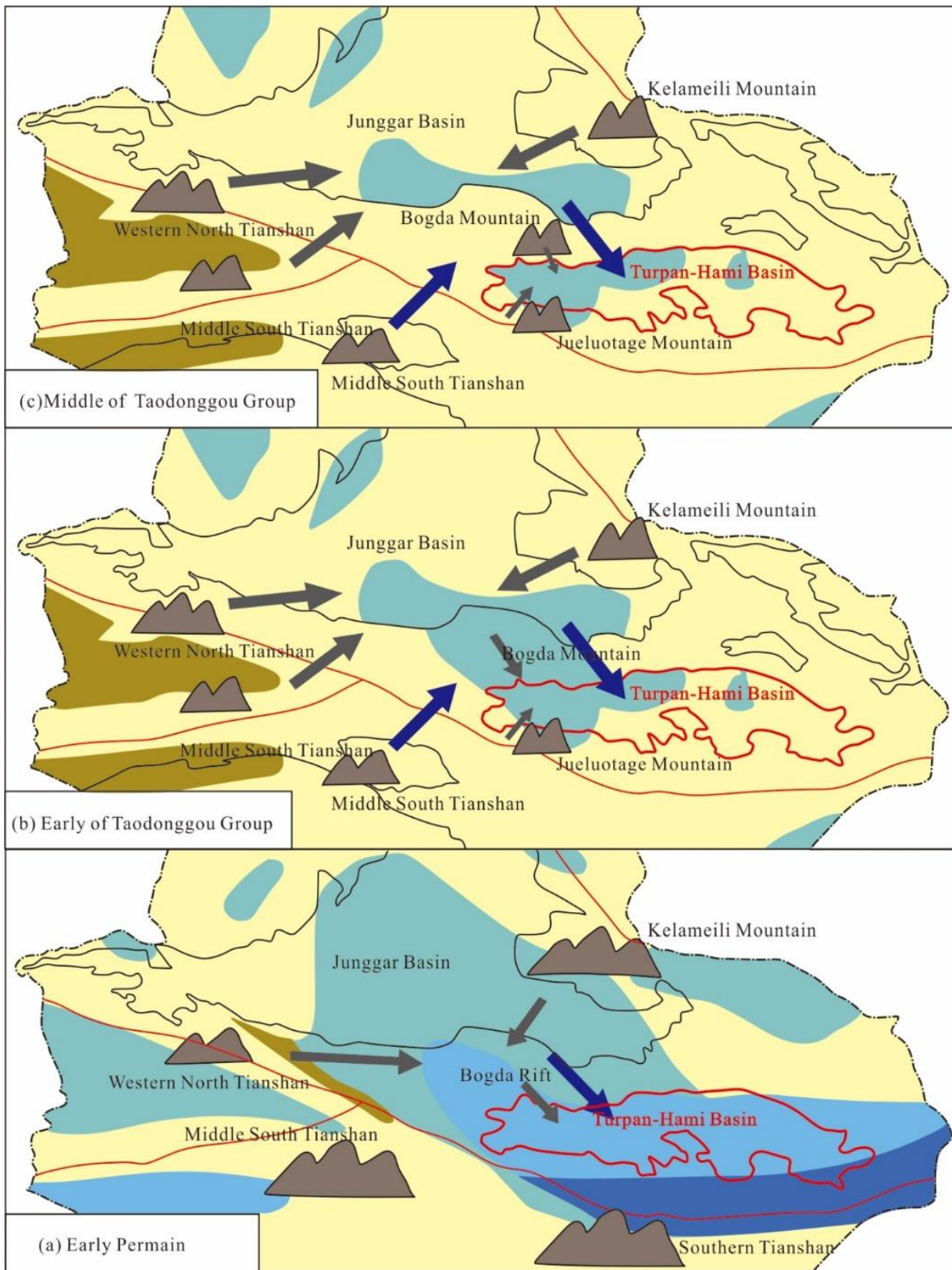
Figure 14: Provenance location from Early Permian to Middle Permian in Tianshan area (modified after Zhao et al., 2020): (a) Early

Permian; (b) Early of Taodonggou Group; (c) Middle to later of Taodonggou Group
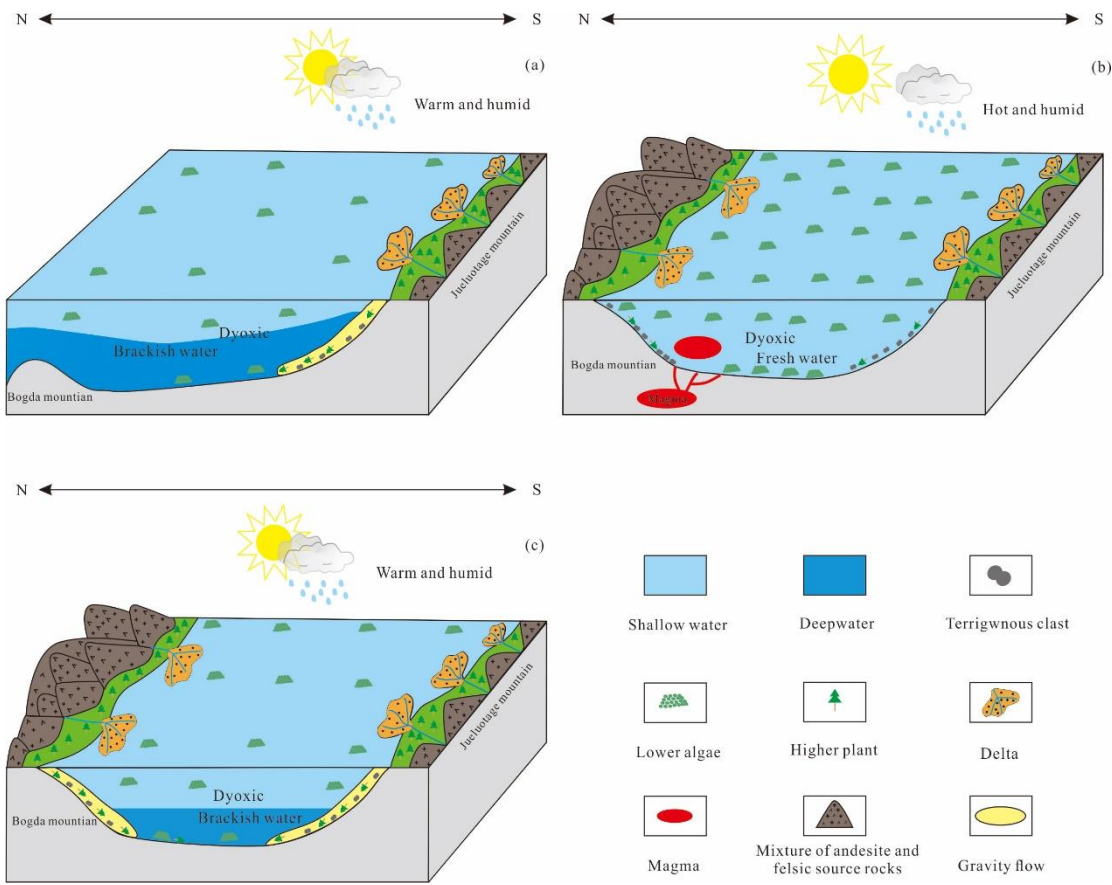
759

760 **Figure 15: Middle Permian source sink system and lake basin evolution history of Turpan-Hami basin: (a) Early Taodonggou Group; (b)**

761 **Middle Taodonggou Group; (c) Late Taodonggou Group**

762 **Appendix**

763 <p align="center">Table.1 Mineral composition of Taodonggou Group mudstone in YT1 well</p>

Samples	Depth/m	Minerals content/%							
		Quartz	K-fledspar	Plagioclace	Calcite	Siderite	Pyrite	Barite	Clay
YT1-1	6084	29.4	0.7	1.8	23.7	/	/	13.3	31.1
YT1-2	6092	30.1	1.1	5.4	26.9	/	/	2.1	34.4
YT1-3	6102	41.9	/	2.5	18.1	/	/	3.2	34.3
YT1-4	6113	35.7	0.5	2.9	10.8	/	/	2.8	47.3
YT1-5	6122	40.5	0.1	2.7	19.4	/	/	4.6	32.7
YT1-6	6129	39.2	0.6	2.1	19.7	/	/	4	34.4
YT1-7	6136	27.9	0.3	0.8	42.8	/	/	4.3	23.9
YT1-8	6140	31.2	0.6	0.6	22.1	/	/	5.6	39.9
YT1-9	6143	34	0.4	0.2	14	/	/	4.5	46.9
YT1-10	6144.7	33.6	2.1	3.7	11.4	2.1	2.8	3.5	40.8
YT1-11	6145.3	37	/	3.7	10.6	1.4	/	2.1	45.2
YT1-12	6145.8	38.4	1.7	2.2	12.5	/	/	3.1	42.1
YT1-13	6147	37.9	/	/	1	/	1.4	1.2	58.5
YT1-14	6151	59.2	0.5	0.2	1.3	/	2.1	/	36.7
YT1-15	6154	21.8	0.8	0.8	1.8	/	/	3.9	70.9
YT1-16	6161	17.2	2.3	4.8	35.4	2	/	5	33.3

764 <p align="center">Table. 2 Major elements of Taodonggou Group mudstone in well YT1</p>

Samples	Depth/m	Content/%										CIA	P/Ti	K_2O/Al_2O_3
		SiO_2	CaO	Al_2O_3	Fe_2O_3	K_2O	TiO_2	Na_2O	MgO	P_2O_5	MnO			
YT1-1	6084	43.79	19.05	11.65	5.32	3	1.35	1.15	1.1	0.9	0.3	68.71	0.49	0.26
YT1-2	6092	54.32	14.01	14.96	6.74	3.39	1.37	1.5	1.34	0.29	0.15	70.1	0.15	0.23
YT1-3	6102	56.63	14.36	11.66	5.42	3.38	1.24	1.23	1.36	0.16	0.19	66.63	0.09	0.29
YT1-4	6113	56.92	7.38	17.52	7.93	4.2	1.28	1.22	1.55	0.21	0.14	72.55	0.12	0.24
YT1-5	6122	51.15	12.62	15.25	7.55	3	1.33	1.2	1.15	0.3	0.34	73.85	0.17	0.20
YT1-6	6129	62.28	4.49	16.07	5.93	3.5	1.15	1.68	0.8	1.17	0.12	70.08	0.74	0.22
YT1-7	6136	52.44	9.31	16.57	8.63	2.54	1.5	1.55	0.66	0.37	0.34	74.57	0.18	0.15
YT1-8	6140	55.37	3.01	21.11	9.64	2.63	1.42	1.5	0.49	0.15	0.24	78.92	0.08	0.12
YT1-9	6143	60.24	2.76	21.27	8.73	1.92	1.76	0.84	0.36	0.23	0.22	85.5	0.09	0.09
YT1-10	6144.7	61.08	2.75	24.16	7.54	0.99	1.82	0.3	0.36	0.21	0.06	93.83	0.08	0.04
YT1-11	6145.3	61.02	2.94	25.39	6.84	0.59	1.84	0.31	0.36	0.26	0.06	95.45	0.10	0.02
YT1-12	6145.8	60.32	5.41	21.32	7.29	0.72	1.85	0.34	0.32	0.21	0.06	93.84	0.08	0.03
YT1-13	6147	60.76	1.83	25.75	7.68	0.68	1.95	0.19	0.35	0.25	0.05	96.07	0.09	0.03
YT1-14	6151	70.11	2.44	12.83	7.28	0.97	1.31	0.34	0.27	0.15	0.05	88.59	0.09	0.08
YT1-15	6154	49.39	1.92	25.41	12.25	2.84	2.87	1.57	0.46	0.15	0.06	80.97	0.04	0.11
YT1-16	6161	43.11	9.56	18.04	14.17	2.83	4.22	1.9	0.77	1.03	0.25	73.12	0.18	0.16

765

Table.3 Characteristics of Trace elements in Taodonggou Group mudstone

Samples		YT1-1	YT1-2	YT1-3	YT1-4	YT1-5	YT1-6	YT1-7	YT1-8	YT1-9	YT1-10	YT1-11	YT1-12	YT1-13	YT1-14	YT1-15	YT1-16
Depth/m		6084	6092	6102	6113	6122	6129	6136	6140	6143	6144.7	6145.3	6145.8	6147	6151	6154	6161
	Be	0.952	1.12	1.67	1	1.52	1.26	1.74	2.17	1.79	1.31	1.35	1.42	0.711	1.77	2.05	1.55
	Sc	9.02	11.9	15.5	11.7	13.6	13.1	15.6	16.2	21.2	11.4	13.2	12.3	7	24	26	17.6
	V	87.3	64.2	72	59.5	106	89.2	100	88.5	88.7	122.3	114.6	131.6	177	145	124	199
	Cr	27.4	21.2	31.8	27.3	40.1	43	40.1	45.1	54.8	48.5	47.6	44.5	43	63	51	40.2
	Co	9.46	12.4	14.9	13.3	11.9	12.6	13.7	18.2	27.6	22.3	21.7	20.6	18.7	24.8	36.9	30.4
	Ni	25.5	27.8	36.7	32.5	32.6	33.2	37.8	37.2	47.5	36.8	35.7	34.6	27.3	41.7	55.4	17.9
	Cu	34.2	33.1	44.8	34.6	51.2	41.8	39.9	50.8	48.9	52.6	50.3	51.4	57.3	55.8	64.4	71.2
	Zn	125	79	92.4	96.1	69.8	90.4	74.4	67.9	78.7	64.6	63.2	65.8	44.1	70.4	114	218
Content/ppm	Ga	17.81	20.1	23.3	19	24.8	21.9	15.1	13.2	16.1	14.5	12.7	13.7	7.14	12.7	19.2	17.3
	Rb	54.5	64.6	73.5	50.4	60	33.5	33.9	16	17.9	15.6	14.6	14.6	13.6	14.2	21	20.7
	Sr	758	357	420	422	291	414	269	151	199	214	244	224	63.9	126	263	393
	Mo	1.29	0.661	0.866	1.24	1.09	1.44	1.17	1.23	2.68	3.02	2.88	3.14	3.86	2.14	1.18	1.28
	Ba	483.83	735.7	633	547.28	159.24	547.66	326.49	465.2	565	503	516	505	427	254	303.56	424.35
	B	46.31	71.3	81.4	67.4	64.5	55.4	60.2	41.3	49.6	44.6	52.6	41.4	41.5	39.7	56.2	54.1
	Th	9.16	6.03	7.31	6.43	8.38	12.4	10.3	10.4	10	9.12	8.33	8.86	6.17	7.32	9.96	3.13
	U	2.13	1.8	1.83	2.14	1.66	3.1	3.17	2.43	2.06	3.1	3.06	2.89	3.2	2.66	2.42	0.73
	Zr	82.7	99.3	124	97.1	107	112	123	132	162	128.8	130.2	123.6	70.8	130.4	192	215
	Hf	2.6	3.77	4.29	3.51	3.87	4.03	4.45	4.76	5.52	4.76	3.94	4.01	2.23	3.21	6.13	6.29
Sr/Ba		1.57	0.49	0.66	0.77	1.83	0.76	0.82	0.32	0.35	0.43	0.47	0.44	0.15	0.5	0.87	0.93
Ga/Rb		0.33	0.31	0.32	0.38	0.41	0.65	0.45	0.83	0.9	0.93	0.87	0.94	0.53	0.89	0.91	0.84
B/Ga		2.6	3.55	3.49	3.55	2.6	2.53	3.99	3.13	3.08	3.08	4.14	3.02	5.81	3.13	2.93	3.13
Rb/K/(10^{-4})		21.87	22.94	26.18	14.45	24.08	11.52	16.07	7.32	11.22	18.97	29.79	24.41	24.08	17.63	8.9	8.81
V/Cr		3.19	3.03	2.26	2.18	2.64	2.07	2.49	1.96	1.62	2.52	2.41	2.96	4.12	2.3	2.43	4.95
V/(V+Ni)		0.77	0.7	0.66	0.65	0.76	0.73	0.73	0.7	0.65	0.77	0.76	0.79	0.87	0.78	0.69	0.92
C		0.22	0.32	0.26	0.54	0.43	0.53	0.61	1.19	1.38	1.61	1.56	1.03	2.42	1.64	1.56	0.93

Table 4 Enrichment Factors of the Taodonggou Group mudstone after AS transformation

Samples	X_{EF}																	
	Be	Sc	V	Cr	Co	Ni	Cu	Zn	Ga	Rb	Sr	Mo	Ba	B	Th	U	Zr	Hf
YT1-1	0.43	0.11	0.92	0.42	0.68	0.51	1.04	1.80	1.28	0.53	3.66	0.63	1.14	0.68	1.05	0.78	0.71	1.28
YT1-2	0.39	0.12	0.53	0.25	0.70	0.44	0.78	0.89	1.13	0.49	1.34	0.25	1.35	0.82	0.54	0.52	0.66	1.44
YT1-3	0.75	0.19	0.76	0.48	1.07	0.74	1.36	1.33	1.68	0.72	2.03	0.43	1.49	1.20	0.83	0.67	1.06	2.11
YT1-4	0.30	0.10	0.42	0.28	0.64	0.43	0.70	0.92	0.91	0.33	1.36	0.41	0.86	0.66	0.49	0.52	0.55	1.15
YT1-5	0.52	0.13	0.85	0.47	0.66	0.50	1.19	0.77	1.37	0.45	1.07	0.41	0.29	0.73	0.73	0.47	0.70	1.45
YT1-6	0.41	0.12	0.68	0.47	0.66	0.48	0.92	0.94	1.14	0.24	1.45	0.51	0.94	0.59	1.03	0.83	0.69	1.44
YT1-7	0.55	0.14	0.74	0.43	0.69	0.53	0.85	0.75	0.77	0.23	0.91	0.40	0.54	0.62	0.83	0.82	0.74	1.54
YT1-8	0.54	0.11	0.51	0.38	0.72	0.41	0.85	0.54	0.52	0.09	0.40	0.33	0.61	0.34	0.66	0.49	0.62	1.29
YT1-9	0.44	0.14	0.51	0.46	1.09	0.52	0.81	0.62	0.64	0.10	0.53	0.72	0.73	0.40	0.63	0.42	0.76	1.49
YT1-10	0.28	0.07	0.62	0.36	0.77	0.36	0.77	0.45	0.50	0.07	0.50	0.72	0.57	0.32	0.50	0.55	0.53	1.13
YT1-11	0.28	0.08	0.55	0.33	0.72	0.33	0.70	0.42	0.42	0.07	0.54	0.65	0.56	0.36	0.44	0.52	0.51	0.89
YT1-12	0.35	0.08	0.76	0.37	0.81	0.38	0.85	0.52	0.54	0.08	0.59	0.84	0.65	0.33	0.55	0.58	0.58	1.08
YT1-13	0.14	0.04	0.84	0.30	0.61	0.25	0.79	0.29	0.23	0.06	0.14	0.86	0.46	0.28	0.32	0.53	0.27	0.50
YT1-14	0.72	0.27	1.39	0.87	1.62	0.76	1.54	0.92	0.83	0.13	0.55	0.95	0.54	0.53	0.76	0.89	1.01	1.43
YT1-15	0.42	0.15	0.60	0.36	1.22	0.51	0.90	0.75	0.63	0.09	0.58	0.27	0.33	0.38	0.52	0.41	0.75	1.38
YT1-16	0.45	0.14	1.35	0.39	1.41	0.23	1.40	2.03	0.81	0.13	1.23	0.41	0.65	0.51	0.23	0.17	1.19	2.00
Average	0.41	0.12	0.73	0.40	0.87	0.44	0.93	0.79	0.75	0.20	0.91	0.56	0.68	0.50	0.59	0.55	0.68	1.29

Table 5 Characteristics of REE in Taodonggou Group mudstone

Samples	Depth/m	Content/ppm																		(La/Yb)$_N$
		La	Ce	Pr	Nd	Sm	Eu	Gd	Tb	Dy	Ho	Er	Tm	Yb	Lu	∑REE	LREE	MREE	HREE	
YT1-1	6084	31.70	57.70	6.73	28.80	5.14	1.46	5.19	0.72	3.89	0.68	2.17	0.30	2.12	0.352	146.953	124.930	17.077	4.946	10.081
YT1-2	6092	27.30	47.80	5.51	22.90	4.79	0.84	4.13	0.73	4.25	0.71	2.40	0.37	2.56	0.408	124.695	103.510	15.447	5.738	7.190
YT1-3	6102	27.30	48.30	5.62	23.10	4.71	1.32	4.17	0.80	4.63	0.88	2.68	0.41	2.89	0.464	127.271	104.320	16.511	6.440	6.369
YT1-4	6113	26.40	45.60	5.20	22.20	4.37	0.96	4.09	0.68	3.88	0.72	2.35	0.36	2.56	0.408	119.783	99.400	14.705	5.678	6.953
YT1-5	6122.	32.60	62.80	7.61	31.70	6.56	1.96	5.77	0.98	5.35	0.97	2.89	0.43	2.92	0.429	162.971	134.710	21.590	6.671	7.527
YT1-6	6129	33.10	80.10	7.48	31.70	6.19	0.62	5.98	0.99	5.58	0.99	3.01	0.50	3.31	0.564	180.108	152.380	20.345	7.383	6.742
YT1-7	6136	33.50	66.40	7.70	31.20	6.19	1.18	5.46	0.91	5.24	0.96	3.05	0.49	3.18	0.454	165.914	138.800	19.936	7.178	7.102
YT1-8	6140	35.90	65.80	7.23	29.20	5.47	1.65	4.96	0.96	5.35	0.96	2.97	0.47	3.01	0.426	164.346	138.130	19.344	6.872	8.041
YT1-9	6143	39.00	73.40	9.60	40.00	7.18	1.44	5.64	1.02	5.91	1.08	3.45	0.52	3.41	0.519	192.169	162.000	22.270	7.899	7.711
YT1-10	6144.7	32.60	66.43	7.34	26.40	6.31	0.98	4.82	0.84	4.97	0.86	3.12	0.33	3.21	0.436	158.646	132.770	18.130	7.096	6.847
YT1-11	6145.3	27.90	62.23	5.23	23.20	5.42	1.04	4.46	0.92	5.41	0.88	2.88	0.44	3.02	0.423	143.453	118.560	17.880	6.763	6.228
YT1-12	6145.8	30.20	65.60	5.64	25.40	5.93	1.02	5.01	0.47	4.54	0.91	2.94	0.46	3.01	0.501	151.631	126.840	5.531	6.911	6.764
YT1-13	6147	8.84	16.80	1.75	6.90	1.39	0.30	1.32	0.27	1.87	0.39	1.27	0.22	1.67	0.265	43.247	34.290	5.531	3.426	3.569
YT1-14	6151	39.40	73.60	8.64	33.60	4.22	1.84	4.32	1.21	5.83	1.03	3.42	0.43	2.98	0.392	180.912	155.240	5.531	7.222	8.914
YT1-15	6154	52.60	105.00	12.30	50.80	9.09	2.45	7.65	1.25	7.14	1.16	3.86	0.57	3.62	0.510	257.997	220.700	28.740	8.557	9.796
YT1-16	6161	39.70	85.70	11.10	52.10	9.76	2.29	8.33	1.34	7.47	1.25	3.75	0.52	3.39	0.502	227.206	188.600	30.440	8.166	7.895

771   LREE = La + Ce + Pr + Nd; MREE = Sm + Eu + Gd + Tb + Dy + Ho; HREE = Er + Tm + Yb + Lu; (La/Yb)$_N$ = (La/Yb)/(La/Yb)$_{chondrite}$